

# Accepted Manuscript

Developing glutathione-activated catechol-type diphenylpolyenes as small molecule-based and mitochondria-targeted prooxidative anticancer theranostic prodrugs

Xia-Zhen Bao, Fang Dai, Qi Wang, Xiao-Ling Jin, Bo Zhou



PII: S0891-5849(18)31521-1

DOI: <https://doi.org/10.1016/j.freeradbiomed.2019.01.033>

Reference: FRB 14131

To appear in: *Free Radical Biology and Medicine*

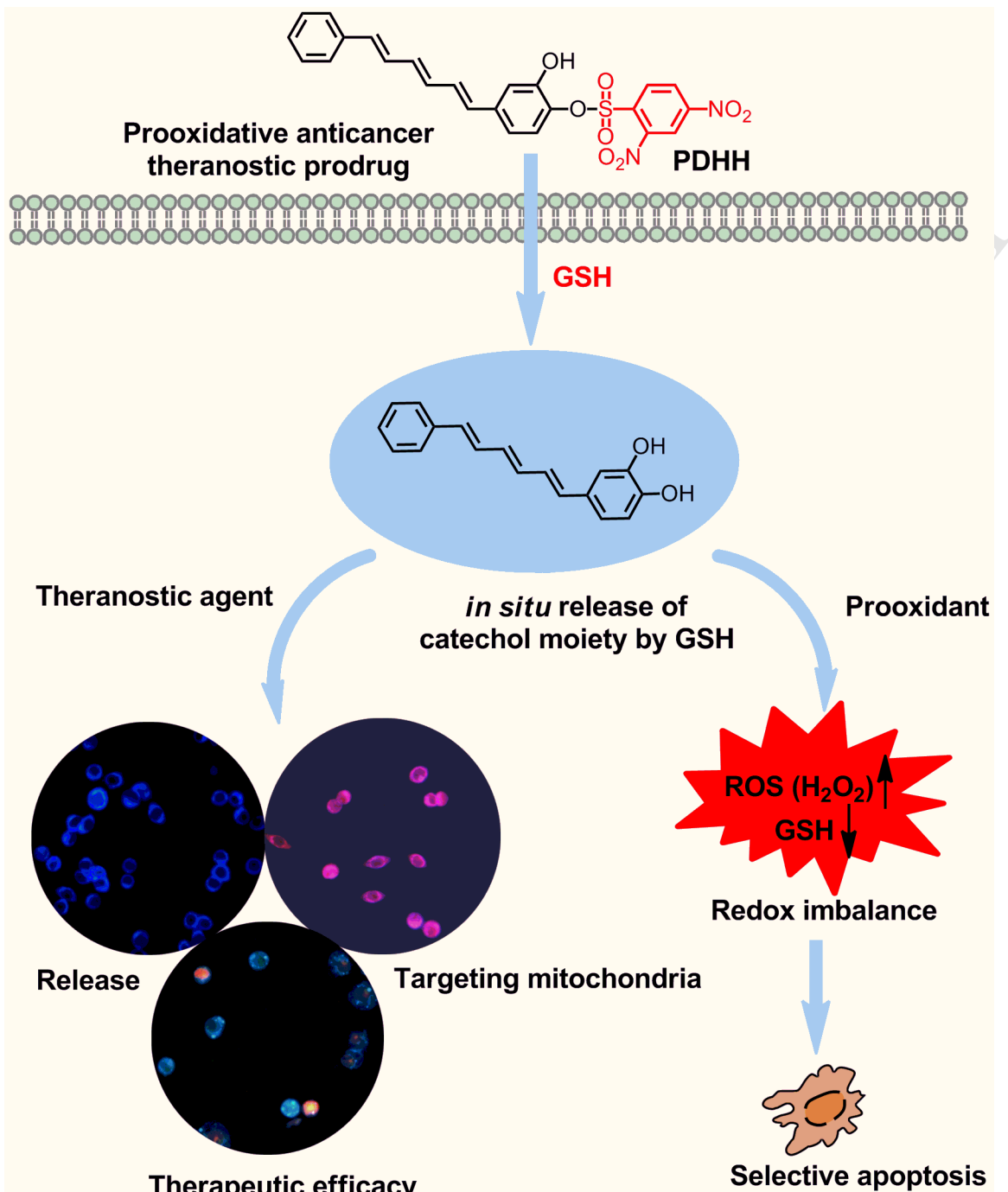
Received Date: 1 September 2018

Revised Date: 24 January 2019

Accepted Date: 24 January 2019

Please cite this article as: X.-Z. Bao, F. Dai, Q. Wang, X.-L. Jin, B. Zhou, Developing glutathione-activated catechol-type diphenylpolyenes as small molecule-based and mitochondria-targeted prooxidative anticancer theranostic prodrugs, *Free Radical Biology and Medicine* (2019), doi: <https://doi.org/10.1016/j.freeradbiomed.2019.01.033>.

This is a PDF file of an unedited manuscript that has been accepted for publication. As a service to our customers we are providing this early version of the manuscript. The manuscript will undergo copyediting, typesetting, and review of the resulting proof before it is published in its final form. Please note that during the production process errors may be discovered which could affect the content, and all legal disclaimers that apply to the journal pertain.



1 **Developing glutathione-activated catechol-type diphenylpolyenes as**  
2 **small molecule-based and mitochondria-targeted prooxidative**  
3 **anticancer theranostic prodrugs**

4 Xia-Zhen Bao, Fang Dai, Qi Wang, Xiao-Ling Jin and Bo Zhou<sup>\*</sup>

5 *State Key Laboratory of Applied Organic Chemistry, Lanzhou University, 222*

6 *Tianshui Street S., Lanzhou, Gansu 730000, China*

7

8

9

10

11

12

13

14

15

16

17

18

19

20

---

21 **\*Corresponding author.**

22 **E-mail:** [bozhou@lzu.edu.cn](mailto:bozhou@lzu.edu.cn)

23 **ABSTRACT**

24 Developing concise theranostic prodrugs is highly desirable for personalized and  
25 precision cancer therapy. Herein we used the glutathione (GSH)-mediated conversion  
26 of 2,4-dinitrobenzenesulfonates to phenols to protect a catechol moiety and developed  
27 stable pro-catechol-type diphenylpolyenes as small molecule-based prooxidative  
28 anticancer theranostic prodrugs. These molecules were synthesized *via* a modular  
29 route allowing creation of various pro-catechol-type diphenylpolyenes. As a typical  
30 representative, PDHH demonstrated three unique advantages: (1) capable of  
31 exploiting increased levels of GSH in cancer cells to *in situ* release a catechol moiety  
32 followed by its *in situ* oxidation to *o*-quinone, leading to preferential redox imbalance  
33 (including generation of H<sub>2</sub>O<sub>2</sub> and depletion of GSH) and final selective killing of  
34 cancer cells over normal cells, and is also superior to 5-fluorouracil and doxorubicin,  
35 the widely used chemotherapy drugs, in terms of its ability to kill preferentially  
36 human colon cancer SW620 cells (IC<sub>50</sub> = 4.3 μM) over human normal liver L02 cells  
37 (IC<sub>50</sub> = 42.3 μM) with a favourable *in vitro* selectivity index of 9.8; (2) permitting a  
38 turn-on fluorescent monitoring for its release, targeting mitochondria and therapeutic  
39 efficacy without the need of introducing additional fluorophores after its activation by  
40 GSH in cancer cells; (3) efficiently targeting mitochondria without the need of  
41 introducing additional mitochondria-directed groups.

42

43 *Keywords:* Glutathione; Diphenylpolyenes; Prooxidant; Theranostic prodrug;  
44 Mitochondria-targeted

45 **1. Introduction**

46 The development of theranostic agents is particularly attractive in the context of  
47 personalized and precision cancer therapy on account of their dual ability to offer both  
48 diagnosis and therapy [1,2]. Prodrugs have also attracted much attention due to their  
49 conversion to toxic species only at the cancer-specific conditions (such as low pH [3],  
50 increased levels of reactive oxygen species (ROS) [4-7], reduced glutathione (GSH)  
51 [8-12] and overexpressed enzymes [13,14]), thereby potentially lacking the dangerous  
52 side effect. With the use of the two concepts, several types of theranostic prodrugs  
53 equipped with fluorophores as optical reporters have been successfully explored to  
54 allow facile monitoring of the release, location and efficacy of anticancer agents [2].  
55 However, they are almost bulky combined systems consist of masked anticancer  
56 drugs, cleavable linkers, fluorophores and cancer targeting ligand. Especially,  
57 additional conjugation of a fluorescent tag is required because most of the anticancer  
58 drugs are intrinsically nonfluorescent. Such modifications might not make sure the  
59 fluorescence is correlated with real location of the drugs once they are released [15].  
60 Therefore, developing small molecule-based anticancer theranostic prodrugs without  
61 the need of introducing additional fluorophores remains a challenge and is highly  
62 desirable to track them and directly visualize their therapeutic effects.

63 Compared with normal cells, cancer cells exhibit aberrant redox homeostasis: on  
64 the one hand, they need increased levels of ROS to maintain their malignant  
65 phenotypes; on the other hand, they survive the ROS stress by upregulating GSH  
66 synthesis [16-19]. The aberrant redox homeostasis illustrates redox Achilles heel of

67 cancer cells [20,21], because as a kind of already stressed cells they are more  
68 vulnerable to further generation of ROS than normal cells [16-19]. Thus, developing  
69 prooxidative anticancer agents (PAAs) capable of generating ROS or/and depleting  
70 GSH has attracted increasing attention [16-19]. Indeed PAAs can preferentially kill  
71 cancer cells over normal cells in this way, but they also increase the ROS amount in  
72 normal cells, leading to side effects [22]. An efficient means to solve the flaw is  
73 designing prooxidative anticancer prodrugs that can be selectively activated by redox  
74 Achilles heel of cancer cells to induce highly selective generation of ROS in cancer  
75 cells, as depicted in Scheme 1A.

76 Catechol moiety, found widely in nature, appears to be an important component to  
77 construct dietary natural products such as piceatannol, green tea polyphenols,  
78 quercetin, caffeic acid, delphinidin, hydroxytyrosol and so on. These catechol-type  
79 molecules usually hold promise in cancer chemoprevention at least in part due to their  
80 prooxidative role based on their oxidative conversion into *o*-quinones during which  
81 ROS are generated [23-29]. However, their oxidative instability also constitutes the  
82 main drawback to use them as anticancer agents.

83 Stilbenes, as the simplest diphenylpolyenes, are a small family of plant secondary  
84 metabolites as exemplified by the most extensively studied resveratrol [30]  
85 pterostilbene and piceatannol. We found previously that among resveratrol and its  
86 hydroxylated analogs, a catechol-type stilbene (3,4-dihydroxy-*trans*-stilbene, DHS) is  
87 the only one that can exploit intracellular copper ions to *in situ* generate its  
88 corresponding *o*-quinone, resulting in activation of nuclear factor erythroid-2 related

89 factor 2 (Nrf2) [26], an important target for cancer chemoprevention. We believe that  
90 further elongating the conjugated links of DHS could facilitate its oxidation to  
91 *o*-quinone and development of the catechol-based PAAs, for example, inserting of  
92 additional double bonds between two aromatic rings to generate various  
93 diphenylpolyenes (Scheme 1B). Nevertheless, this modification will intensify their  
94 instability, a bottleneck in practical use of catechol molecules as mentioned above.

95 **Scheme 1 here**

96

97 In our opinion, the bottleneck could be solved by designing pro-catechols that is  
98 usually robust but can be *in situ* activated to catechols under cancer-specific  
99 conditions, such as increased levels of GSH observed in cancer cells [31,32]. It is  
100 well-established that 2,4-dinitrobenzenesulfonates (DNBS) are easily subject to  
101 nucleophilic attack by thiols including GSH followed by exposure of a free phenolic  
102 hydroxyl group [33]. This reaction prompts the development in designing fluorescent  
103 probes for thiols [34,35], GSH-activated photosensitizers for selective photodynamic  
104 action [36,37] and thiols-triggered anticancer prodrug [38]. However, this reaction, to  
105 date, has not been used for protecting a catechol moiety.

106 As part of our effort to develop natural product-inspired PAAs for targeting redox  
107 Achilles heel of cancer cells [26-29, 39-43], herein we used the above GSH-mediated  
108 conversion of DNBS to phenols as a general strategy to design a variety of  
109 pro-catechol-type diphenylpolyenes (PDHS, PDHB and PDHH differentiated by  
110 various numbers of double bonds between two aromatic rings, Scheme 1B and

111 Scheme 2) as new-style theranostic prodrugs. Specifically, the 4-OH on their catechol  
112 moieties was selectively blocked by DNBS since this hydroxyl is more reactive than  
113 3-OH. We reasoned that the masked 4-OH could be activated by GSH in cancer cells  
114 to *in situ* release a catechol moiety, while maintaining its salient feature in normal  
115 cells; the resulting catechol moiety allows its *in situ* oxidation to *o*-quinone, leading to  
116 generation of ROS and final selective killing of cancer cells (Scheme 1B). The  
117 designed diphenylpolyenes also serve as the reporters of their release, location and  
118 therapeutic efficacy because their fluorescence is mostly quenched by attachment of a  
119 strong electron withdrawing DNBS, but once they are activated by GSH in cancer  
120 cells, permitting a turn-on fluorescent monitoring. Moreover, the DNBS works as a  
121 cleavable linker under a cancer-specific condition (increased levels of GSH), the total  
122 theranostic prodrug system is thereby very concise. Unexpectedly, the  
123 organelle-specific delivery was found in the case of diphenylpolyenes which were  
124 efficiently localized within mitochondria, providing novel mitochondria-directed  
125 groups that would facilitate developing mitochondria-targeted fluorescence probes  
126 and drugs.

127

## 128 **2. Materials and methods**

### 129 *2.1. Materials*

130 Leibovitz's L-15 Medium (L-15), Roswell Park Memorial Institute (RPMI)-1640,  
131 Dulbecco's Modified Eagle Medium (DMEM), Minimum Essential Media (MEM),  
132 3-(4,5-dimethylthiazol-2-yl)-2,5-diphenyltetrazolium bromide (MTT), bovine serum

133 albumin (BSA), dihydroethidium (DHE), propidium iodide (PI), rhodamine 123, yeast  
134 glutathione reductase (GR), 2-vinylpyridine (97%), reduced L-glutathione (GSH),  
135 oxidized L-glutathione (GSSG), L-buthionine-(S,R)-sulfoximine (BSO), catalase  
136 from bovine liver (CAT), DL-dithiothreitol (DTT) and 5,  
137 5'-dithiobis-2-nitrobenzoic acid (DTNB), glutathione S-transferase (GST) from equine  
138 liver, ethacrynic acid (EA) and carbonyl cyanide  
139 4-(trifluoromethoxy)phenylhydrazone (FCCP) were purchased from Sigma-Aldrich  
140 (St. Louis, MO, USA). Mito-Tracker Deep Red and Amplex™ Red Hydrogen  
141 Peroxide/Peroxidase Assay Kit were purchased from Thermo Fisher Scientific  
142 (Waltham, USA). Annexin V-FITC Apoptosis Detection Kit was from BD (Becton,  
143 Dickinson and Company). Nicotinamide adenine dinucleotide 2'-phosphate reduced  
144 tetrasodium salt (NADPH) was from Roche Diagnostics GmbH (Mannheim,  
145 Germany). ER-Tracker Red, Lyso-Tracker Red and bicinchoninic acid (BCA) protein  
146 assay kit were from Beyotime Institute of Biotechnology (Jiangsu, China).

147

148 *2.2. Synthesis of the catechols and the pro-catechols*

149 The synthesis details of the catechols and the pro-catechols were shown in the  
150 Supplemental Information. These compounds were characterized with  $^1\text{H}$  NMR,  $^{13}\text{C}$   
151 NMR and HRMS spectra, and their purity was further checked by HPLC-based  
152 analyses.

153

154 *2.3. Stability assay*

155 Stability of the catechols and pro-catechols in PBS/DMSO (1/1, v/v, pH 7.4) at  
156 room temperature was monitored at their maximum absorbance for 10 h (at 30 min  
157 intervals) by using a UV/visible spectrophotometer. Additionally, their stability was  
158 further validated using HPLC-based analyses. Specifically, the solutions were  
159 prepared by dissolving the catechols or the pro-catechols in PBS/DMSO (1/1, v/v) to  
160 a final concentration of 160  $\mu$ M, then were maintained at room temperature for  
161 different periods of time for HPLC analysis using a Waters HPLC system equipped  
162 with a Sun Fire<sup>TM</sup>, C-18 column (4.6 mm  $\times$  150 mm). H<sub>2</sub>O (eluent A)/CH<sub>3</sub>CN (eluent  
163 B) was used as the mobile phase. The temperature of the column was maintained at 35  
164 °C and the flow rate of the mobile phase was 1.0 mL/min. The run was set as follows:  
165 for PDHS A(H<sub>2</sub>O): B(CH<sub>3</sub>CN) = 0.45:0.55, for PDHB A(H<sub>2</sub>O): B(CH<sub>3</sub>CN) = 0.4:0.6,  
166 for PDHH A(H<sub>2</sub>O): B(CH<sub>3</sub>CN) = 0.35:0.65.

167

168 *2.4. HPLC-based analyses for in vitro activation of the pro-catechols by GSH*

169 The ability of the pro-catechols to release its parent catechols in the presence of  
170 GSH at ambient temperature was evaluated using a Waters HPLC system equipped  
171 with a Sun Fire<sup>TM</sup>, C-18 column (4.6 mm  $\times$  150 mm). After adding GSH (1.6 mM) to  
172 a solution of pro-catechols (160  $\mu$ M) in CH<sub>3</sub>CN/H<sub>2</sub>O (1/1, v/v), the products at  
173 different periods of time (1, 3, 6, 9 and 12 h) were examined by HPLC. The  
174 experimental conditions were the same as those described in the stability assay using  
175 HPLC.

176

177 *2.5. Fluorometric analysis for in vitro activation of the pro-catechols by GSH*

178       Fluorescence spectroscopic studies were carried out at room temperature on a LS  
179       55 Luminescence Spectrometer (PerkinElmer). The catechols and the pro-catechols  
180       were dissolved in DMSO to make a 3 mM stock solution, which was diluted to 1  $\mu$ M  
181       as testing solution in PBS/DMSO (8/2, v/v) for measurement.

182

183 *2.6. Kinetic analysis for in vitro activation of the pro-catechols by GSH*

184       The reactions of the pro-catechols (5  $\mu$ M) with GSH (0.25, 0.5 and 1 mM) were  
185       carried out in PBS/DMSO (v/v, 1/1) under pseudo-first-order conditions at 37 °C in  
186       the absence or presence of equine liver GST (0.03 mg/mL). The increased  
187       fluorescence due to the production of the catechols, was monitored within 1 h using  
188       TECAN Infinite M200 multimode microplate reader (For DHS,  $\lambda_{ex}$  = 330 nm,  $\lambda_{em}$  =  
189       410 nm; For DHB,  $\lambda_{ex}$  = 350 nm,  $\lambda_{em}$  = 440 nm; For DHH,  $\lambda_{ex}$  = 370 nm,  $\lambda_{em}$  =  
190       475 nm). The second-order rate constants ( $k_2$ ) were obtained by plotting the  
191       pseudo-first-order constants versus the corresponding GSH concentration.

192

193 *2.7. Cell culture*

194       Human colon cancer SW620, malignant melanoma A375, ovarian cancer SKOV3,  
195       and fibrosarcoma HT-1080 cells as well as normal cells including human liver L02,  
196       human umbilical vein endothelial HUVEC and mouse hippocampal neuronal HT-22  
197       cells were obtained from the Shanghai Institute of Biochemistry and Cell Biology,  
198       Chinese Academy of Sciences. SW620 cells were incubated in L15 medium

199 supplemented with 10% Newborn Calf Serum (NCS) and gentamycin sulfate (50  
200 µg/L); A375 and HT-22 cells were cultured in DMEM supplemented with 10% NCS,  
201 NaHCO<sub>3</sub> (3.7 g/L), L-Glutamine (0.2 g/L) and antibiotics (penicillin/streptomycin,  
202 100 kU/L); SKOV3, L02 and HUVEC cells were cultured in RPMI-1640  
203 supplemented with 10% fetal bovine serum (FBS), NaHCO<sub>3</sub> (2 g/L) and antibiotics  
204 (penicillin/streptomycin, 100 kU/L); HT-1080 cells was grown in MEM supplemented  
205 with 10% (v/v) FBS, penicillin (100 kU/L), streptomycin (100 kU/L), NaHCO<sub>3</sub> (2.2  
206 g/L) and sodium pyruvate (0.11 g/L). The cells were maintained in a humidified  
207 incubator in 5% CO<sub>2</sub>/95% air at 37 °C and the exponentially growing cells were used  
208 for all experiments.

209

#### 210 2.8. MTT assays

211 Cells were plated in flat-bottomed 96-well plates ( $2 \times 10^4$  cells/well for SW620,  
212  $4 \times 10^3$  cells/well for A375, SKOV3, HT-1080, L02, HUVEC and HT-22) and  
213 incubated at 37 °C for 24 h. The cells were treated with the tested compounds at  
214 varying concentrations and incubated for 48 h at 37 °C. In the case of inhibition, the  
215 cells were pretreated with DTT (400 µM), CAT (0.5 mg/mL) or EA (10 µM) for 1 h  
216 before adding the tested compounds. After 48 h exposure, medium was replaced by  
217 100 µL of MTT solution (0.5 mg/mL in PBS) and incubation for another 4 h. The  
218 MTT medium was aspirated and substituted with 100 µL DMSO. UV-vis absorbance  
219 was measured at 570 nm using a microplate reader (Bio-Rad M680 ELISA).  
220 Experiments were performed each in sextuplicate and repeated three times.

221    2.9. *Fluorescence imaging for subcellular distribution and therapeutic efficacy*

222    SW620 and L02 cells were seeded into 6-well plates at  $4 \times 10^5$  cells/well and  
223    cultured at 37 °C with 5% CO<sub>2</sub> for 24 h. The cells were incubated with PDHH (5 μM)  
224    for 1, 2 and 3 h. In the case of inhibition, SW620 cells were pretreated with BSO (1  
225    mM) for 1 h before incubation with PDHH. For determining the subcellular  
226    distribution of the catechols and the pro-catechols, SW620 cells were incubated with  
227    the tested compounds for 3 h. Then the cells were washed with PBS followed by  
228    incubation with Mito-Tracker Deep Red (1.0 μM), ER-Tracker Red (1 μM) or  
229    Lyso-Tracker Red (1 μM) for another 30 min. For monitoring the death of SW620  
230    cells induced by PDHH, the cells were treated with PDHH (15 μM) for 9, 12, 18 and  
231    24 h, then the cells were collected and labeled with PI (5 μg/mL) for 30 min. All the  
232    cells were washed by PBS buffer before imaging. The fluorescence images were  
233    acquired by microscope Leica DM 400B (Leica Microsystems CMS GmbH, Wetzlar,  
234    Germany). All experimental parameters (exposure time, objective lens) remained  
235    unchanged when the different fluorescence images were captured.

236

237    2.10. *Fluorescence imaging for generation of intracellular ROS*

238    SW620 cells and L02 cells were seeded onto 6-well plates at  $4 \times 10^5$  cells/well. After  
239    24 h, the cells were incubated with 5 μM PDHH for 6 h or 9 h. Then the cells were  
240    rinsed with PBS for 2-3 times and stained with 3 μM DHE for additional 30 min at  
241    37°C. Then the cells were washed by PBS buffer before imaging. The fluorescence  
242    images were acquired by microscope Leica DM 4000B (Leica Microsystems CMS

243 GmbH, Wetzlar, Germany) with a $\times$ 40 objective lens.

244

245 *2.11. Measuring H<sub>2</sub>O<sub>2</sub> released from SW620 cells*

246 SW620 ( $2\times10^4$  cells/well) cells were seeded in 96-well plates overnight and the  
247 medium was replaced by Krebs-Ringer phosphate (KRPG) buffer before the cells  
248 were treated with PDHH (2 and 5  $\mu$ M) for 6 and 9 h in the absence or presence of 1 h  
249 pretreatment with CAT. Aliquots of medium were taken out and their H<sub>2</sub>O<sub>2</sub> levels  
250 were determined using the Amplex<sup>TM</sup> Red Hydrogen Peroxide/Peroxidase Assay Kit  
251 [44]. Specifically, 20  $\mu$ L of medium was added into 100  $\mu$ L of reaction mixture  
252 (containing 50  $\mu$ M Amplex Red reagent and 0.1 U/mL HRP in KRPG buffer),  
253 warmed at 37 °C for ten minutes, and then subjected to fluorescence analysis on a  
254 TECAN Infinite M200 multimode microplate reader ( $\lambda_{ex}$  = 530 nm,  $\lambda_{em}$  = 590 nm)  
255 with 20  $\mu$ L of KRPG buffer as the negative control [44].

256

257 *2.12. Detection of intracellular GSH levels*

258 SW620 ( $4\times10^5$  cells/well) and L02 ( $4\times10^5$  cells/well) cells were seeded in 6-well  
259 plates in growth medium (2 mL) and then incubated at 37°C in a 5% carbon dioxide  
260 atmosphere. Intracellular GSH contents were evaluated using the glutathione  
261 reductase-DTNB recycling assay [45], and the related details were described in our  
262 previous paper [43].

263 *2.13. Measurement of mitochondrial membrane potential*

264 SW620 and L02 cells were seeded onto 6-well plates at a density of  $4 \times 10^5$  cells per  
265 well and then incubated with FCCP or PDHH for the 18 and 24 h. The cells without  
266 treatment were used as the control. After incubation, the cells were trypsinized and  
267 washed with PBS followed by staining with 5  $\mu$ M of rhodamine-123 for additional 30  
268 min at 37°C. After washing again with PBS, the cells were analyzed using  
269 FACSCanto flow cytometer (Becton Dickinson, San Jose, CA, USA). The mean  
270 fluorescence was determined by counting 10,000 events.

271

#### 272 *2.14. Apoptosis analysis*

273 SW620 ( $4 \times 10^5$  cells/well) and L02 ( $4 \times 10^5$  cells/well) cells were seeded on each  
274 well of a six-well plate and allowed to grow overnight. Medium was changed and the  
275 cells were treated with serial concentrations of PDHH for 48 h at 37 °C. Then the  
276 cells were trypsinized, washed repeatedly with PBS for three times and centrifuged at  
277 350 g for 5 min. The cells were resuspended in 100  $\mu$ L 1×Annexin V binding buffer,  
278 labeled with 5  $\mu$ L annexin V-FITC/PI from the detection kit (Becton Dickinson, San  
279 Jose, CA, USA), and incubated for 15 min at room temperature. After incubation, 400  
280  $\mu$ L of 1×Annexin V binding buffer was added to each sample prior to analyses on the  
281 FACSCanto flow cytometer (Becton Dickinson, San Jose, CA, USA). A total of  
282  $1.0 \times 10^4$  events were counted for each sample.

283

#### 284 *2.15. Statistical analysis*

285 Data are expressed as the mean  $\pm$  SD. Statistical comparisons among the results

286 were performed using analysis of variance. Significant differences ( $P < 0.05$ ) between  
287 the means of two groups were analyzed by Student's t-test.

288

289

290 **3. Results and discussion**

291 *3.1. Synthesis of the diphenylpolyenes*

292 The designed diphenylpolyenes were synthesized according to the optimized routes  
293 as outlined in Scheme 2. The requisite aldehyde **2** was obtained by a sequential  
294 protection of the 4- and 3-OH of 3,4-dihydroxybenzaldehyde using  
295 *t*-butyldimethylsilyl (TBS) and methoxymethyl (MOM) ethers, respectively. Another  
296 key intermediate benzylphosphonate **6** was prepared from the conjugate carboxylic  
297 acid *via* esterification, reduction, bromination and nucleophilic substitution. With the  
298 intermediates **2** and **6** in hand, the key Witting-Hornor reaction was explored under  
299 various alkaline conditions (including NaH/THF, MeONa/DMF, LDA/THF and  
300 *t*-BuOK/DMF). The reaction proceeded smoothly only in *t*-BuOK/DMF, giving  
301 surprisingly the product **7** with deprotection of TBS in moderate yield. To the best of  
302 our knowledge, this is the first use of *t*-BuOK to complete one-step  
303 Witting-Hornor/selective-deprotection of TBS reaction. Treatment of **7** with  
304 2,4-dinitrobenzenesulfonyl chloride in DCM and Et<sub>3</sub>N followed by deprotection of  
305 MOM under the con. HCl condition afforded finally the designed diphenylpolyenes **9**  
306 (PDHS, PDHB and PDHH) in overall yields of 30.5, 16.5 and 14.6 %, respectively.  
307 Noticeably, the total synthesis was accomplished *via* a modular route allowing

308 creation of various pro-catechol-type diphenylpolyenes. In addition, the  
309 2,4-dinitrobenzenesulfonyl group was added at the final stage of the synthesis, so that  
310 this synthesis procedure may be applied to create other protecting group onto the  
311 catecholic 4-OH.

312 **Schemes 2-3 here**

313

314 *3.2. Stability analysis*

315 The stability of the catechols and pro-catechols was first evaluated by monitoring  
316 their UV/Vis absorption changes in PBS/DMSO (1:1, v/v) at ambient temperature (see  
317 Supplementary Figure S1). Figure 1A and B shows the changes in absorbance at  
318 maximum as a function of the incubation time. The catechols (DHS, DHB and DHH)  
319 were less stable due to their oxidative susceptibility, as suggested by their gradual  
320 decay over time, and their decay rates were increased as elongation of the conjugated  
321 links. In contrast, the pro-catechols (PDHS, PDHB and PDHH) showed almost no  
322 signs of decay in PBS for 10 h, highlighting their improving oxidative stability by  
323 blocking the 4-OH. The stability was also further validated by HPLC-based analyses  
324 (Figure 1C and D). Also, the pro-catechols demonstrated significantly better stability  
325 than the catechols. Noticeably, the pro-catechols showed a handful of decay probably  
326 owing to their hydrolysis to the catechols. The decay was not observed based on  
327 UV-visible spectral analyses because the pro-catechols and the catechols exhibited  
328 almost identical absorbance characteristics.

329 **Figure 1 here**

330

331    *3.3. In vitro activation of pro-catechols by GSH*

332    The *in vitro* activation of the pro-catechols by GSH was next monitored using  
333    HPLC-based analyses. Addition of 10 equiv. of GSH to a solution of PDHH in  
334    CH<sub>3</sub>CN/water (1/1, v/v) induced a decrease in its peak intensity at 14.69 min  
335    accompanied by the appearance of a new chromatographic peak at 4.77 min  
336    corresponding to the formation of DHH (Figure 2). Similar activation was also  
337    observed in the case of PDHS and PDHB (Figure 2). It should be pointed out that the  
338    build-up of the catechols is not completely correlated with the decay of the  
339    procatechins due to oxidative instability of the former (Figure 2B, D and F).

340

**Figure 2 here**

341

342    The *in vitro* activation of the pro-catechols was also checked by fluorescence  
343    analyses. As expected, the pro-catechols compared with the parent catechols exhibited  
344    a very weak fluorescence emission in PBS/DMSO (8:2, v/v) but the signals were  
345    significantly increased over time upon adding GSH, suggesting a turn-on fluorescence  
346    response (Figure 3). Furthermore, the fluorescence emission spectra generated by the  
347    reaction of pro-catechols with GSH were consistent with those of the corresponding  
348    catechols (Figure S2), supporting strongly activation of the pro-catechols to the  
349    corresponding catechols by GSH. It is also noticeable that the degradation of the most  
350    unstable DHH within 1 h in PBS/DMSO (v/v, 1:1) at 37 °C was almost completely  
351    inhibited by a large excess of GSH (Figure S3). This facilitates the investigation on

352 the reaction kinetics of the pro-catechols with GSH based on the increased  
353 fluorescence emission of the resulting catechols. Consequently, we used the  
354 pseudo-first-order conditions to determine the second-order rate constants ( $k_2$ ) of the  
355 pro-catechols with GSH, by using a multimode microplate reader. Plotting the  
356 pseudo-first-order rate constants ( $k_{obs}$ ) against the GSH concentrations gave the  
357 straight lines with an intercept above the zero point, indicating a possible more  
358 complex kinetics (Figure 4). On the basis of the  $k_2$  values (Table 1) obtained from the  
359 straight lines, the reactivity of the pro-catechols with GSH follows the sequence of  
360 PDHH > PDHB > PDHS, highlighting that the reactivity was increased as elongation  
361 of the conjugated links. Considering that glutathione S-transferases (GSTs) as phase II  
362 detoxification enzymes catalyze the nucleophilic attack by GSH on non-polar  
363 electrophilic molecules [46], we also compared the  $k_2$  values in the absence and  
364 presence of equine liver GST to clarify its contribution on the activation of  
365 pro-catechols by GSH. It can be seen from Table 1 that the presence of GST enhanced  
366 moderately the  $k_2$  values of PDHB and PDHS, and failed to do this in the case of  
367 PDHH, suggesting that they are not efficient substrates of GST. Taken together, the  
368 above HPLC and fluorescence data support strongly the activation of the  
369 pro-catechols by GSH to release the corresponding catechols.

370 **Figures 3 and 4 and Table 1 here**

371

372 *3.4. Cytotoxicity and structure-activity relationship*

373 Subsequently, MTT assay was performed to assess the cytotoxicity of all tested

374 molecules towards various cancer cells (human colon cancer SW620, malignant  
375 melanoma A375, ovarian cancer SKOV3 and fibrosarcoma HT-1080 cells) and  
376 normal cells (human liver L02, human umbilical vein endothelial HUVEC and mouse  
377 hippocampal neuronal HT-22 cells). The IC<sub>50</sub> values derived from the titration curves  
378 (Figure S4) are listed in Table 2 and allowed us to identify the following  
379 structure-activity relationships: (1) the cytotoxicity was obviously increased as  
380 elongation of the conjugated links in both the catechols and pro-catechols, in line with  
381 their ability to facilitate the formation of *o*-quinone; (2) the pro-catechols exhibited  
382 higher cytotoxicity and better selectivity than the corresponding catechols with PDHH  
383 being the most active one among the tested molecules; For example, in SW620 and  
384 L-02 cells, IC<sub>50</sub> values of PDHH were determined as 4.3 and 42.3 μM (selectivity  
385 index: 9.8), whereas those of DHH were 9.4 and 33.2 μM, respectively; (3) noticeably,  
386 PDHH was superior to 5-fluorouracil and doxorubicin, the widely used chemotherapy  
387 drugs, in the ability to kill preferentially SW620 over normal L-02 cells with a  
388 favourable *in vitro* selectivity index of 9.8.

389 **Table 2 here**

390  
391 3.5. Visualization for the selective activation of PDHH by GSH in SW620 cells over  
392 normal L02 cells

393 The increased selective cytotoxicity of the pro-catechols compared with the  
394 corresponding catechols are in tune with their improving stability and hint at the  
395 possibility that they could be selectively activated by GSH in cancer cells to *in situ*

396 release the catechol moiety. To further clarify this point, we selected the most active  
397 PDHH to observe its selective activation in live SW620 cells over normal L02 cells  
398 by fluorescence imaging. After incubation of SW620 cells with PDHH, we observed a  
399 gradual increased bright-blue fluorescence signal over time (Figure 5A-D). However,  
400 this signal was significantly abrogated by pretreatment of the cells with  
401 L-buthionine-sulfoximine (BSO) for 1 h (Figure 5E), a GSH synthase inhibitor,  
402 confirming that activation of PDHH is GSH-dependent. In comparison, only faint  
403 activation of PDHH occurred in L02 cells after 6 h incubation (Figure 5F-I). The  
404 significant difference in activating PDHH between SW620 and L02 cells is a result of  
405 their different basal levels of GSH [31,32], and also the reason why PDHH could kill  
406 preferentially SW620 over L-02 cells. This is further supported from our determined  
407 basal levels of GSH of SW620 and L02 cells ( $122 \pm 1.92$  and  $29 \pm 3.18$  nmol/mg  
408 protein, respectively) by the glutathione reductase-DTNB recycling assay [45]. In  
409 other words, the 4.2-fold difference in the basal levels of GSH between the two cell  
410 lines might be enough for making the selective cytotoxicity of PDHH (selectivity  
411 index: 9.8). More importantly, in line with the abrogation of the fluorescence signal,  
412 pretreatment of SW620 cells with BSO for 1 h decreased significantly the basal  
413 levels of GSH from the original  $122 \pm 1.92$  to  $55 \pm 2.92$  nmol/mg protein.

414 **Figure 5 here**

415  
416 GST is often overexpressed in numerous cancer cells and contributes to resistance  
417 of cancer cells towards cytostatic drugs by catalyzing their conjugation with GSH [46].

418 To clarify whether GST is involved in the activation of PDHH by GSH and  
419 contributes to its selective cytotoxicity, we further checked the effect of ethacrynic  
420 acid (EA, a GST inhibitor) on the cytotoxicity of PDHH against SW620 cells. As  
421 illustrated in Figure S5, pretreatment of SW620 cells with EA had no appreciable  
422 effect on the cytotoxicity of PDHH. This is consistent with the kinetic results showing  
423 that GST has no impact on the reaction of PDHH with GSH (Table 1), and further  
424 supports that the selective cytotoxicity of PDHH is caused by the difference of GSH  
425 levels, rather than that of GST levels, between SW620 and L02 cells. Furthermore,  
426 previous research has revealed that uptake of resveratrol, a hydroxylated stilbene, by  
427 human hepatocytes is similar to that obtained in human hepatoma HepG2 cells [47].  
428 So that we speculated that the selectivity observed in the case of PDHH as the same  
429 diphenylpolyene with resveratrol is not due to the differential cellular uptake.  
430 According to the above results, we can conclude that PDHH can be selectively  
431 activated by increased levels of GSH in SW620 cells to *in situ* release a catechol  
432 moiety, resulting in its selective cytotoxicity, and its activation can be visualized by a  
433 “turn-on” blue fluorescence response. In addition, it should be emphasized that the  
434 byproducts generated in the activation of PDHH by GSH, SO<sub>2</sub> and (2,4-dinitrophenyl)  
435 glutathione, were non-cytotoxic, as described previously [39].

436

### 437 3.6. Visualization for the subcellular distribution of PDHH after activation

438 To determine the subcellular distribution of PDHH after activation, co-localization  
439 experiments were performed. SW620 cells were co-stained with PDHH and

440 commercially available Mito-Tracker Deep Red, ER-Tracker Red or Lyso-Tracker  
441 Red. As shown in Figure 6, PDHH was gradually activated in SW620 cells over the  
442 course of 3 h and the blue fluorescence signal at the time points of 3 h was  
443 well-overlapped with the red fluorescence signal from Mito-Tracker Deep Red with  
444 the Pearson's correlation coefficient being 0.997. In comparison, the Pearson's  
445 correlation coefficients were determined as 0.548 and 0.377 with ER-Tracker Red and  
446 Lyso-Tracker Red, respectively (Figure S6). These results indicate clearly that after  
447 activation PDHH is selectively localized in mitochondria, known as the major site of  
448 cellular ROS production and regulators of apoptosis. Similar mitochondrial  
449 localization was also observed in its parent catechol DHH (Figure S7). Consequently  
450 there are two possibilities of either activation of PDHH to DHH by cytoplasmic GSH  
451 followed by localization of DHH to mitochondria or localization of PDHH to  
452 mitochondria followed by its activation to DHH by mitochondrial GSH. Additionally,  
453 the mitochondrial localization was also observed in the case of PDHB, PDHS and  
454 their corresponding catechols (DHB and DHS), even in the case of DPHE (Scheme 2)  
455 bearing no any phenolic hydroxyl group (Figure S7). To our knowledge, this is the  
456 first report of the diphenylpolyene skeletons capable of selectively targeting  
457 mitochondria without the need of additional introducing mitochondria-directed groups  
458 such as the widely used triphenylphosphonium [48-51].

459 **Figure 6 here**

460

461 *3.7. Visualization for therapeutic efficacy of PDHH*

462 PDHH was further used to monitor SW620 cell death together with propidium  
463 iodide (PI), a widely used nuclear fluorescent dye for late apoptotic cells. To induce  
464 rapid cell death, SW620 cells were exposed to 15 µM PDHH for different time points.  
465 As the incubation time increased, PI entered gradually the cells and stained the nuclei,  
466 resulting in a strong red fluorescence signal in the nuclei region, which is indicative of  
467 the occurrence of late cell apoptosis (Figure 7). In contrast, after treatment with  
468 PDHH for 24 h, the cells demonstrated additional typical characteristics of cell  
469 apoptosis including shrinkage of cytoplasm along with formation of vacuoles and  
470 apoptotic bodies (Figure 7), highlighting its superiority in monitoring late cell  
471 apoptosis.

472 **Figure 7 here**

473

474 *3.8. Prooxidative role of PDHH*

475 Having established the theranostic role of PDHH for its release, location and  
476 therapeutic efficacy, we turned our attention to clarify whether its prooxidative role is  
477 responsible for its ability to preferentially kill SW620 cells over L-02 cells. It is  
478 known that under aerobic conditions, catechols are usually unstable and easily  
479 converted into its *o*-quinone intermediates *via* two-electron oxidation along with  
480 generation of ROS from the oxidation [23-29] (see also Figure 8A). Additionally, the  
481 *o*-quinone intermediates are the Michael acceptor-type electrophiles, which could be  
482 conjugated with intracellular nucleophilic GSH, leading to depletion of GSH and  
483 intracellular generation of ROS [52] (see also Figure 8A). Therefore, ROS derived

484 from the oxidation of catechols mediate usually their anticancer activity [23-29].

485 The involvement of ROS (mainly including H<sub>2</sub>O<sub>2</sub>) in the cytotoxicity of PDHH

486 against SW620 cells is supported from significant cytotoxic revision (Figure 8B) by

487 DTT (a sulphydryl-containing nucleophile capable of quenching electrophilic *o*-quinone

488 and ROS) and CAT (a specific scavenger of H<sub>2</sub>O<sub>2</sub>). To clarify the production of the

489 *o*-quinone of DHH and its quenching by DTT, we investigated its Cu(II)-induced

490 UV/Vis absorption changes under aerobic conditions. Addition of Cu(II) to DHH in

491 CH<sub>3</sub>CN/water (1/1, v/v) caused a rapid decrease of its absorption peak centered at 362

492 nm along with an immediate appearance of a new band in the range of 400-700 nm

493 due to the production of the *o*-quinone of DHH (Figure 8C). The new band decreased

494 promptly with the time extended, implying that the *o*-quinone of DHH is very labile

495 (the inset in Figure 8C). Meanwhile, the new band can be smoothed by adding DTT,

496 supporting strongly the quenching of the *o*-quinone (Figure 8C).

497 The cytotoxic revision by CAT hints at the role H<sub>2</sub>O<sub>2</sub> in the cytotoxicity of PDHH,

498 we thus used conjunctively a fluorescence probe DHE and CAT to imagine the

499 intracellular generation of H<sub>2</sub>O<sub>2</sub> in living SW620 cells. The probe emits red

500 fluorescence upon its reaction with superoxide and other oxidants (e.g., iron and H<sub>2</sub>O<sub>2</sub>,

501 cytochrome c and H<sub>2</sub>O<sub>2</sub>) [53, 54]. Upon treatment of SW620 cells with PDHH for 6 or

502 9 h, the red fluorescence appeared in SW620 cells, but not in L-02 cells, and the

503 increased red fluorescence in SW620 cells was significantly revised by CAT (Figure

504 8D). Noticeably, SW620 cells were almost intact based on the treatment with PDHH

505 for 9 h (Figure S8), thereby ruling out the possibility that cytochrome c released from

mitochondria into cytosol would catalyze the reaction of DHE with H<sub>2</sub>O<sub>2</sub>. The above results correlated well with the reversion of CAT on the cytotoxicity (Figure 8B) to further support the intracellular generation of H<sub>2</sub>O<sub>2</sub> in SW620 cells treated with PDHH. It should be pointed out that CAT is not membrane-permeable due to its large molecular size, but as a neutral small molecule H<sub>2</sub>O<sub>2</sub> can diffuse across cell membranes [55] and CAT retained extracellularly can scavenge H<sub>2</sub>O<sub>2</sub> diffused from inside cells to reduce intracellular H<sub>2</sub>O<sub>2</sub> and to thereby revise the cytotoxicity of PDHH. This also indicates that significant amounts of H<sub>2</sub>O<sub>2</sub> leaks into the culture media. Therefore, we further carried out the Amplex Red assay [44] to clarify this point. As illustrated in 8E, treatment with PDHH induced dose- and time-dependently the H<sub>2</sub>O<sub>2</sub> release from SW620 cells, which was significantly inhibited by CAT, providing a direct proof for the generation of H<sub>2</sub>O<sub>2</sub> induced by PDHH.

The increased H<sub>2</sub>O<sub>2</sub> was also associated with dose- and time-dependent decrease of GSH (Figure 8F) (another important indicator of redox status), suggesting that PDHH induces redox imbalance of SW620 cells. To identify whether PDHH induces collapse of mitochondrial membrane potential of SW620 cells, we subsequently performed the rhodamine 123 experiment in combination with using FCCP (a mitochondrial uncoupler) as the control [56]. As shown in Figure 9A, treatment with either FCCP or PDHH decreased the fluorescence intensity of rhodamine 123. The above results demonstrate that the probe works in the normal and not in the quenching (increased fluorescence) mode [56], and PDHH induces collapse of mitochondrial membrane potential of SW620 cells.

528 The redox imbalance and subsequent collapse of mitochondrial membrane potential  
529 facilitated final apoptosis of SW620 cells (Figure 10A). This was supported by  
530 reversion of CAT and DTT on redox imbalance such as accumulation of H<sub>2</sub>O<sub>2</sub> (Figure  
531 8D and E) and depletion of GSH (Figure 8F), collapse of mitochondrial membrane  
532 potential (Figure 9A) and apoptosis (Figure 10A) of SW620 cells, induced by PDHH.  
533 In a sharp contrast, PDHH failed to induce the redox imbalance (Figure 8D and F),  
534 collapse of mitochondrial membrane potential (Figure 9B) and apoptosis in L-02 cells  
535 (Figure 10B). The above results provide an entire evidence chain to support that  
536 PDHH works as a PAA after its activation to DHH by GSH in SW620 cells.

537 **Figures 8-10 here**

538

539 In summary, we used the GSH-mediated conversion of DNBS to phenols to protect  
540 a catechol moiety and designed stable pro-catechol-type diphenylpolyenes as small  
541 molecule-based anticancer theranostic prodrugs. The designed molecules were  
542 synthesized *via* a modular route allowing creation of various pro-catechol-type  
543 diphenylpolyenes and introduction of other protecting group onto the catecholic 4-OH.  
544 Dissimilar to the currently available theranostic prodrugs, the designed PDHH is a  
545 concise molecule permitting a turn-on fluorescent monitoring for its release, targeting  
546 mitochondria and therapeutic efficacy. As a potent PAA, PDHH is capable of  
547 exploiting increased levels of GSH in cancer cells to *in situ* release a catechol moiety  
548 followed by its *in situ* oxidation to toxic *o*-quinone, leading to preferential redox  
549 imbalance (including depletion of GSH and generation of H<sub>2</sub>O<sub>2</sub>) and final selective

550 apoptosis of cancer cells over normal cells. It is also superior to 5-fluorouracil and  
551 doxorubicin, the widely used chemotherapy drugs, in terms of its ability to kill  
552 preferentially SW620 over normal L-02 cells. Additionally, we identified the  
553 diphenylpolyene skeletons as novel mitochondria-directed groups that should prove  
554 useful for creating new mitochondria-targeted fluorescence probes and drugs.

555

556

557 **Acknowledgments**

558 This work was supported by the National Natural Science Foundation of China  
559 (Grant No. 21672091)

560

561 **Appendix A. Supplementary material**

562 Supplementary data associated with this article can be found in the online version  
563 at <http://dx.doi.org/10.1016/j.freeradbiomed>.

564

565

566

567

568

569

570

571 **References**

- 572 [1]. E. S. Andersen, M. Dong, M. M. Nielsen, K. Jahn, R. Subramani, W.  
573 Mamdouh, M. M. Golas, B. Sander, H. Stark, C. L. P. Oliveira, J. S. Pedersen,  
574 V. Birkedal, F. Besenbacher, K. V. Gothelf, J. Kjems, Self-assembly of a  
575 nanoscale DNA box with a controllable lid, *Nature* 459 (2009) 73-76.
- 576 [2]. M. H. Lee, A. Sharma, M. J. Chang, J. Lee, S. Son, J. L. Sessler, C. Kang, J. S.  
577 Kim, Fluorogenic reaction-based prodrug conjugates as targeted cancer  
578 theranostics, *Chem. Soc. Rev.* 47 (2018) 28-52.
- 579 [3]. J.-Z. Du, X.-J. Du, C.-Q. Mao, J. Wang, Tailor-made dual pH-sensitive  
580 polymer-doxorubicin nanoparticles for efficient anticancer drug delivery, *J.  
581 Am. Chem. Soc.* 133 (2011) 17560-17563.
- 582 [4]. J. L. Major Jourden, S. M. Cohen, Hydrogen peroxide activated matrix  
583 metalloproteinase inhibitors: a prodrug approach, *Angew. Chem. Int. Ed.* 49  
584 (2010) 6795-6797.
- 585 [5]. Y. Kuang, K. Balakrishnan, V. Gandhi, X. Peng, Hydrogen peroxide inducible  
586 DNA cross-linking agents: targeted anticancer prodrugs, *J. Am. Chem. Soc.* 133  
587 (2011) 19278-19281.
- 588 [6]. E.-J. Kim, S. Bhuniya, H. Lee, H. M. Kim, C. Cheong, S. Maiti, K. S. Hong, J.  
589 S. Kim, An activatable prodrug for the treatment of metastatic tumors, *J. Am.  
590 Chem. Soc.* 136 (2014) 13888-13894.
- 591 [7]. R. Kumar, J. Han, H.-J. Lim, W. X. Ren, J.-Y. Lim, J.-H. Kim, J. S. Kim,  
592 Mitochondrial induced and self-monitored intrinsic apoptosis by antitumor  
593 theranostic prodrug: in vivo imaging and precise cancer treatment, *J. Am.*

- 594 Chem. Soc. 136 (2014) 17836-17843.
- 595 [8]. M. Ye, X. Wang, J. Tang, Z. Guo, Y. Shen, H. Tian, W.-H. Zhu, Dual-channel  
596 NIR activatable theranostic prodrug for in vivo spatiotemporal tracking  
597 thiol-triggered chemotherapy, Chem. Sci. 7 (2016) 4958-4965.
- 598 [9]. F. Kong, Z. Liang, D. Luan, X. Liu, K. Xu, B. Tang, A glutathione  
599 (GSH)-responsive near-infrared (NIR) theranostic prodrug for cancer therapy  
600 and imaging, Anal. Chem. 88 (2016) 6450-6456.
- 601 [10]. X. Wu, X. Sun, Z. Guo, J. Tang, Y. Shen, T. D. James, H. Tian, W. Zhu, In  
602 vivo and in situ tracking cancer chemotherapy by highly photostable NIR  
603 fluorescent theranostic prodrug, J. Am. Chem. Soc. 136 (2014) 3579-3588.
- 604 [11]. S. Bhuniya, S. Maiti, E.-J. Kim, H. Lee, J. L. Sessler, K. S. Hong, J. S. Kim,  
605 An activatable theranostic for targeted cancer therapy and imaging, Angew.  
606 Chem. Int. Ed. 53 (2014) 4469-4474.
- 607 [12]. S. Santra, C. Kaittanis, O. J. Santiesteban, J. M. Perez, Cell-specific,  
608 activatable, and theranostic prodrug for dual-targeted cancer imaging and  
609 therapy, J. Am. Chem. Soc. 133 (2011) 16680-16688.
- 610 [13]. Y. Ichikawa, M. Kamiya, F. Obata, M. Miura, T. Terai, T. Komatsu, T. Ueno, K.  
611 Hanaoka, T. Nagano, Y. Urano, Selective ablation of  
612  $\beta$ -galactosidase-expressing cells with a rationally designed activatable  
613 photosensitizer, Angew. Chem. Int. Ed. 53 (2014) 6772-6775.
- 614 [14]. G. Zheng, J. Chen, K. Stefflova, M. Jarvi, H. Li, B. C. Wilson, Photodynamic  
615 molecular beacon as an activatable photosensitizer based on

- 616 protease-controlled singlet oxygen quenching and activation, Proc. Natl. Acad.  
617 Sci. U. S. A. 104 (2007) 8989-8994.
- 618 [15]. Q. Hu, M. Gao, G. Feng, B. Liu, Mitochondria-targeted cancer therapy using a  
619 light-up probe with aggregation-induced-emission characteristics, Angew.  
620 Chem. Int. Ed. 53 (2014) 14225-14229.
- 621 [16]. D. Trachootham, J. Alexandre, P. Huang, Targeting cancer cells by  
622 ROS-mediated mechanisms: a radical therapeutic approach?, Nat. Rev. Drug  
623 Discov. 8 (2009) 579-591.
- 624 [17]. L. L. Policastro, I. L. Ibañez, C. Notcovich, H. A. Duran, O. L. Podhajcer, The  
625 tumor microenvironment: characterization, redox considerations, and novel  
626 approaches for reactive oxygen species-targeted gene therapy, Antioxid.  
627 Redox Signal. 19 (2013) 854-895.
- 628 [18]. C. Martín-Cordero, A. José León-González, J. Manuel Calderón-Montaño, E.  
629 Burgos-Morón, M. López-Lázaro, Pro-oxidant natural products as anticancer  
630 agents, Curr. Drug Targets 13 (2012) 1006-1028.
- 631 [19]. C. Gorrini, I. S. Harris, T. W. Mak, Modulation of oxidative stress as an  
632 anticancer strategy, Nat. Rev. Drug Discov. 12 (2013) 931-947.
- 633 [20]. X. Cui, Reactive oxygen species: the Achilles' Heel of cancer cells?, Antioxid.  
634 Redox Signal. 16 (2012) 1212-1214.
- 635 [21]. J. P. Fruehauf, V. Trapp, Reactive oxygen species: an Achilles' heel of  
636 melanoma?, Expert. Rev. Anticancer Ther. 8 (2008) 1751-1757.
- 637 [22]. J. R. Totter, Spontaneous cancer and its possible relationship to oxygen

- 638 metabolism, Proc. Natl. Acad. Sci. U. S. A. 77 (1980) 1763-1767.
- 639 [23]. J. G. Liehr, D. Roy, Free radical generation by redox cycling of estrogens,  
640 Free Radic. Biol. Med. 8 (1990) 415-423.
- 641 [24]. A. M. Samuni, E. Y. Chuang, M. C. Krishna, W. Stein, W. DeGraff, A. Russo,  
642 J. B. Mitchell, Semiquinone radical intermediate in catecholic  
643 estrogen-mediated cytotoxicity and mutagenesis: Chemoprevention strategies  
644 with antioxidants, Proc. Natl. Acad. Sci. U. S. A. 100 (2003) 5390-5395.
- 645 [25]. M. E. Haque, M. Asanuma, Y. Higashi, I. Miyazaki, K.-i. Tanaka, N. Ogawa,  
646 Apoptosis-inducing neurotoxicity of dopamine and its metabolites via reactive  
647 quinone generation in neuroblastoma cells, BBA - General Subjects 1619  
648 (2003) 39-52.
- 649 [26]. D. Lin, F. Dai, L.-D. Sun, B. Zhou, Toward an understanding of the role of a  
650 catechol moiety in cancer chemoprevention: The case of copper- and  
651 *o*-quinone-dependent Nrf2 activation by a catechol-type resveratrol analog,  
652 Mol. Nutr. Food Res. 59 (2015) 2395-2406.
- 653 [27]. F. Dai, Q. Wang, G.-J. Fan, Y.-T. Du, B. Zhou, ROS-driven and preferential  
654 killing of HepG2 over L-02 cells by a short-term cooperation of Cu(II) and a  
655 catechol-type resveratrol analog, Food Chem. 250 (2018) 213-220.
- 656 [28]. Y.-H. Wang, F. Dai, B. Zhou, A catechol-type resveratrol analog manifests  
657 antiangiogenic action by constructing an efficient catalytic redox cycle with  
658 intracellular copper ions and NQO1, Mol. Nutr. Food Res. 62 (2018) 1700969.
- 659 [29]. F. Dai, Y.-T. Du, Y.-L. Zheng, B. Zhou, A promising redox cycle-based

- strategy for designing a catechol-type diphenylbutadiene as a potent prooxidative anti-melanoma agent, *Free Radic. Biol. Med.* 2018, DOI: <https://doi.org/10.1016/j.freeradbiomed.2018.11.018>.
- [30]. J. A. Baur, D. A. Sinclair, Therapeutic potential of resveratrol: the *in vivo* evidence, *Nat. Rev. Drug Discov.* 5 (2006) 493-506.
- [31]. S. K. Biswas, I. Rahman, Environmental toxicity, redox signaling and lung inflammation: The role of glutathione, *Mol. Aspects Med.* 30 (2009) 60-76.
- [32]. K. Umezawa, M. Yoshida, M. Kamiya, T. Yamasoba, Y. Urano, Rational design of reversible fluorescent probes for live-cell imaging and quantification of fast glutathione dynamics, *Nat. Chem.* 9 (2016) 279-286.
- [33]. H. Maeda, H. Matsuno, M. Ushida, K. Katayama, K. Saeki, N. Itoh, 2,4-Dinitrobenzenesulfonyl fluoresceins as fluorescent alternatives to Ellman's reagent in thiol-quantification enzyme assays, *Angew. Chem. Int. Ed.* 44 (2005) 2922-2925.
- [34]. S. Ji, H. Guo, X. Yuan, X. Li, H. Ding, P. Gao, C. Zhao, W. Wu, W. Wu, J. Zhao, A highly selective OFF-ON red-emitting phosphorescent thiol probe with large stokes shift and long luminescent lifetime, *Org. Lett.* 12 (2010) 2876-2879.
- [35]. J. Zhang, A. Shibata, M. Ito, S. Shuto, Y. Ito, B. Mannervik, H. Abe, R. Morgenstern, Synthesis and characterization of a series of highly fluorogenic substrates for glutathione transferases, a general strategy, *J. Am. Chem. Soc.* 133 (2011) 14109-14119.

- 682 [36]. I. S. Turan, F. P. Cakmak, D. C. Yildirim, R. Cetin-Atalay, E. U. Akkaya,  
683 Near-IR absorbing BODIPY derivatives as glutathione-activated  
684 photosensitizers for selective photodynamic action, *Chem. Eur. J.* 20 (2014)  
685 16088-16092.
- 686 [37]. H. He, P.-C. Lo, D. K. P. Ng, A glutathione-activated phthalocyanine-based  
687 photosensitizer for photodynamic therapy, *Chem. Eur. J.* 20 (2014) 6241-6245.
- 688 [38]. Y. Xu, J. Chen, Y. Li, S. Peng, X. Gu, M. Sun, K. Gao, J. Fang, Synthesis and  
689 biological studies of the thiols-triggered anticancer prodrug for a more  
690 effective cancer therapy, *Org. Biomol. Chem.* 13 (2015) 2634-2639.
- 691 [39]. X.-Z. Bao, F. Dai, X.-R. Li, B. Zhou, Targeting redox vulnerability of cancer  
692 cells by prooxidative intervention of a glutathione-activated Cu(II)  
693 pro-ionophore: Hitting three birds with one stone, *Free Radic. Biol. Med.* 124  
694 (2018) 342-352.
- 695 [40]. F. Dai, C.-H. Yuan, Y. Ji, Y.-T. Du, X.-Z. Bao, L.-X. Wu, X.-L. Jin, B. Zhou,  
696 Keto-enol-based modification on piperlongumine to generate a potent Cu(II)  
697 ionophore that triggers redox imbalance and death of HepG2 cells, *Free Radic.*  
698 *Biol. Med.* 120 (2018) 124-132.
- 699 [41]. F. Dai, W.-J. Yan, Y.-T. Du, X.-Z. Bao, X.-Z. Li, B. Zhou, Structural basis,  
700 chemical driving forces and biological implications of flavones as Cu(II)  
701 ionophores, *Free Radic. Biol. Med.* 108 (2017) 554-563.
- 702 [42]. W.-J. Yan, Q. Wang, C.-H. Yuan, F. Wang, Y. Ji, F. Dai, X.-L. Jin, B. Zhou,  
703 Designing piperlongumine-directed anticancer agents by an

- 704       electrophilicity-based prooxidant strategy: A mechanistic investigation, Free  
705       Radic. Biol. Med. 97 (2016) 109-123.

706       [43]. F. Dai, G.-Y. Liu, Y. Li, W.-J. Yan, Q. Wang, J. Yang, D.-L. Lu, D.-J. Ding, D.  
707       Lin, B. Zhou, Insights into the importance for designing curcumin-inspired  
708       anticancer agents by a prooxidant strategy: The case of diarylpentanoids, Free  
709       Radic. Biol. Med. 85 (2015) 127-137.

710       [44]. J. G. Mohanty, J. S. Jaffe, E. S. Schulman, D. G. Raible, A highly sensitive  
711       fluorescent micro-assay of H<sub>2</sub>O<sub>2</sub> release from activated human leukocytes  
712       using a dihydroxyphenoxazine derivative, J. Immunol. Methods 202 (1997)  
713       133-141.

714       [45]. C. Vandeputte, I. Guizon, I. Genestie-Denis, B. Vannier, G. Lorenzon, A  
715       microtiter plate assay for total glutathione and glutathione disulfide contents in  
716       cultured/isolated cells: performance study of a new miniaturized protocol, Cell  
717       Biol. Toxicol. 10 (1994) 415-421.

718       [46]. D. M. Townsend, K. D. Tew, The role of glutathione-S-transferase in  
719       anti-cancer drug resistance, Oncogene 22 (2002) 7369.

720       [47]. A. Lançon, D. Delma, H. Osman, J. P. Thénot, B. J. N. Latruffe, Human  
721       hepatic cell uptake of resveratrol: involvement of both passive diffusion and  
722       carrier-mediated process, Biochem. Biophys. Res. Co. 316 (2004) 1132-1137.

723       [48]. A. T. Hoye, J. E. Davoren, P. Wipf, M. P. Fink, V. E. Kagan, Targeting  
724       mitochondria, Acc. Chem. Res. 41 (2008) 87-97.

725       [49]. M. F. Ross, G. F. Kelso, F. H. Blaikie, A. M. James, H. M. Cochemé, A.

- 726 Filipovska, T. Da Ros, T. R. Hurd, R. A. J. Smith, M. P. Murphy, Lipophilic  
727 triphenylphosphonium cations as tools in mitochondrial bioenergetics and  
728 free radical biology, Biochemistry (Moscow) 70 (2005) 222-230.
- 729 [50]. M. P. Murphy, R. A. J. Smith, Targeting antioxidants to mitochondria by  
730 conjugation to lipophilic cations, Annu. Rev. Pharmacol. Toxicol. 47 (2007)  
731 629-656.
- 732 [51]. J. Zielonka, J. Joseph, A. Sikora, M. Hardy, O. Ouari, J. Vasquez-Vivar, G.  
733 Cheng, M. Lopez, B. Kalyanaraman, Mitochondria-targeted  
734 triphenylphosphonium-based compounds: syntheses, mechanisms of action,  
735 and therapeutic and diagnostic applications, Chem. Rev. 117 (2017)  
736 10043-10120.
- 737 [52]. A. Felim, A. Urios, A. Neudörffer, G. Herrera, M. Blanco, M. Largeron,  
738 Bacterial plate assays and electrochemical methods: an efficient tandem for  
739 evaluating the ability of catechol-thioether metabolites of MDMA (“Ecstasy”)  
740 to induce toxic effects through redox-cycling, Chem. Res. Toxicol. 20 (2007)  
741 685-693.
- 742 [53]. F. R. M. Laurindo, D. C. Fernandes, C. X. C. Santos, Assessment of  
743 superoxide production and NADPH oxidase activity by HPLC analysis of  
744 dihydroethidium oxidation products, Method. Enzymol. 441 (2008) 237-260.
- 745 [54]. B. Kalyanaraman, V. Darley-Usmar, K. J. A. Davies, P. A. Dennery, H. J.  
746 Forman, M. B. Grisham, G. E. Mann, K. Moore, L. J. Roberts, H.  
747 Ischiropoulos, Measuring reactive oxygen and nitrogen species with

748 fluorescent probes: challenges and limitations, Free Radic. Biol. Med. 52

749 (2012) 1-6.

750 [55]. F. Antunes, E. Cadenas, Estimation of H<sub>2</sub>O<sub>2</sub> gradients across biomembranes,

751 FEBS Lett. 475 (2000) 121-126.

752 [56]. S. W. Perry, J. P. Norman, J. Barbieri, E. B. Brown, H. A. Gelbard,

753 Mitochondrial membrane potential probes and the proton gradient: a practical

754 usage guide, BioTechniques 50 (2011) 98-115.

755

756

757

758

759

760

761

762

763

764

765

766

767

768

769

770

771 **Table 1** Second-order rate constants ( $k_2$ ) for the reaction of the pro-catechols with  
772 GSH at 37 °C.<sup>a</sup>

Compounds	$k_2$ (M <sup>-1</sup> s <sup>-1</sup> )	$k_2$ (M <sup>-1</sup> s <sup>-1</sup> ) <sup>b</sup>
PDHS	0.67 ± 0.02	0.76 ± 0.03
PDHB	0.79 ± 0.02	0.86 ± 0.05
PDHH	0.85 ± 0.04	0.90 ± 0.03

773 <sup>a</sup> The reaction of the pro-catechols with GSH was carried out in PBS/DMSO (1:1, v:v)  
774 under pseudo-first-order conditions at 37 °C.

775 <sup>b</sup> The  $k_2$  values were determined in the presence of equine liver GST.

776

777

778 **Table 2.** Cytotoxicity of the catechols and the pro-catechols against various cancer cells (SW620, A375, SKOV3 and HT-1080) and normal  
 779 cells (L02, HUVEC and HT-22)<sup>[a]</sup>

Compounds	IC <sub>50</sub> (μM)						
	SW620	A375	SKOV3	HT-1080	L02	HUVEC	HT-22
DHS	43.2 ± 3.14	24.8 ± 0.35	43.6 ± 2.02	17.6 ± 1.10	>100	>100	15.9 ± 1.35
PDHS	11.6 ± 1.06	16.4 ± 0.36	26.6 ± 1.25	14.9 ± 0.83	51.2 ± 0.12	67.8 ± 0.86	34.6 ± 2.95
DHB	19.5 ± 1.92	17.1 ± 1.13	36.7 ± 0.85	10.9 ± 0.84	68.2 ± 1.26	64.1 ± 2.54	3.57 ± 0.92
PDHB	6.8 ± 0.72	13.2 ± 1.56	14.2 ± 1.28	13.1 ± 0.95	50.4 ± 0.26	55.4 ± 1.37	28.3 ± 0.78
DHH	9.4 ± 0.63	14.6 ± 1.32	28.9 ± 0.92	9.1 ± 1.21	33.2 ± 2.02	50.6 ± 1.86	1.5 ± 2.01
PDHH	4.3 ± 0.83	11.1 ± 1.62	10.8 ± 2.38	8.7 ± 0.53	42.3 ± 1.06	49.1 ± 2.01	21.3 ± 0.92
5-Fluorouracil	14.6 ± 0.21				40.3 ± 2.01	58.0 ± 1.44	33.3 ± 2.89
Doxorubicin	3.41 ± 0.02				0.12 ± 1.01	0.38 ± 0.56	1.14 ± 0.02

780 [a] Values for IC<sub>50</sub> were assayed after 48 h of treatment and are presented as means ± SD for at least three independent experiments.

781 **Figure legends**

782

783 **Scheme 1.** (A) Designing concept of prooxidative anticancer prodrugs for inducing  
784 highly selective ROS generation in cancer cells over normal cells. Prooxidative  
785 anticancer prodrugs can be activated to PAAs by redox Achilles heel of cancer cells,  
786 and the resulting PAAs induce selectively redox imbalance (including generation of  
787 ROS and depletion of GSH) of cancer cells, leading to their preferential killing. (B)  
788 Diagrammatic representation of designing the glutathione-activated catechol-type  
789 diphenylpolyenes as small molecule-based prooxidative anticancer theranostic  
790 prodrugs.

791

792 **Scheme 2.** The structures and abbreviations for the catechols and the pro-catechols  
793 investigated .

794

795 **Scheme 3.** Synthesis of the pro-catechols **9** (PDHS, PDHB and PDHH) and their  
796 parent catechols **10** (DHS, DHB and DHH). Reagents and reaction conditions: (a)  
797 TBSCl, imidazole, DMF, r.t., 2 h; (b) MOMCl, DIPEA, DCM, 2 h; (c) con. H<sub>2</sub>SO<sub>4</sub>,  
798 MeOH, reflux, 18 h; (d) DIBAL-H, DCM, -78 - 0°C, 4 h; (e) PBr<sub>3</sub>, Et<sub>2</sub>O, 0°C - r.t. 1 h;  
799 (f) triethylphosphite, 140°C, 6 h; (g) 2, *t*-BuOK, DMF, 0°C - r.t. overnight; (h)  
800 2,4-dinitrobenzenesulfonyl chloride, TEA, DCM, reflux, 6 h; (i) con. HCl, MeOH,  
801 reflux, 6 h; (j) con. HCl, MeOH, r.t., 6 h. TBSCl = tert-butyldimethylsilyl chloride;  
802 DMF = N,N-dimethylformamide; MOMCl = chloromethyl methyl ether; DIPEA =

803 N,N-diisopropylethylamine; DCM = dichloromethane; DIBAL-H = diisobutyl  
804 aluminium hydride; PBr<sub>3</sub> = phosphorus tribromide; Et<sub>2</sub>O = ether; *t*-BuOK = potassium  
805 tert-butylate; TEA = triethylamine.

806

807 **Figure 1** Stability analyses of the catechols and the pro-catechols in PBS/DMSO (1:1,  
808 v/v, pH 7.4) by UV/vis absorption spectroscopy (A and B) and HPLC (C and D). 35  
809 μM DHS and PDHS, 20 μM DHB and PDHB, as well as 15 μM DHH and PDHH  
810 were used in the spectrum-based analyses; The catechols and the pro-catechols (160  
811 μM) were used in the HPLC-based analyses.

812

813 **Figure 2** Reverse-phase HPLC chromatogram analyses for the reaction of PDHS (A),  
814 PDHB (C) or PDHH (E) with GSH in CH<sub>3</sub>CN/H<sub>2</sub>O (1/1, v/v) at ambient temperature.  
815 a: GSH (1.6 mM); b: the catechols (160 μM); c: the pro-catechols (160 μM); d-h: the  
816 reaction solution of pro-catechols (160 μM) with GSH (1.6 mM) for 1, 3, 6, 9 and 12  
817 h, respectively. The detection wavelengths of DHS, DHB and DHH were set as 335  
818 344, and 366 nm, respectively. Figure B, D and F shows the changes in the  
819 concentrations of the pro-catechols and the catechol products as a function of time.

820

821 **Figure 3** Time-dependent fluorescence spectral changes of the pro-catechols (1.0 μM)  
822 induced by 10 equiv. of GSH in PBS/DMSO (8:2, v/v) at ambient temperature (A-C).  
823 a: the pro-catechols, b-f: the reaction solution of pro-catechols with GSH for 1, 3, 6, 9  
824 and 12 h, respectively. The inset shows the dependence of the fluorescence intensity

825 on incubation time. For DHS,  $\lambda_{\text{ex}} = 330 \text{ nm}$ ,  $\lambda_{\text{em}} = 410 \text{ nm}$ ; For DHB,  $\lambda_{\text{ex}} = 350 \text{ nm}$ ,  
826  $\lambda_{\text{em}} = 440 \text{ nm}$ ; For DHH,  $\lambda_{\text{ex}} = 370 \text{ nm}$ ,  $\lambda_{\text{em}} = 475 \text{ nm}$ .

827

828 **Figure 4** Plots of the pseudo-first-order rate constants  $k_{\text{obs}}$  of pro-catechols versus the  
829 initial GSH concentrations in PBS/DMSO (1/1, v/v) in the absence (A) or presence of  
830 equine liver GST (B).

831

832 **Figure 5** Fluorescence imaging for *in situ* selective activation of PDHH by GSH in  
833 SW620 cells (A-E) over in L-02 cells (F-I). The cells were incubated with PDHH (5  
834  $\mu\text{M}$ ) for 0.5 (A, F), 1 (B, G), 3 (C, H) and 6 (D, I) h. (E) SW620 cells were pretreated  
835 with BSO (1 mM) for 1 h and then incubated with PDHH for another 3 h. For PDHH,  
836 an excitation wavelength  $\lambda_{\text{ex}} = 340\text{-}380 \text{ nm}$  and  $\lambda_{\text{em}} = \text{LP } 425 \text{ nm}$  were used. Scale  
837 bar = 20  $\mu\text{m}$ .

838

839 **Figure 6** Fluorescence imaging analyses for localization of PDHH to mitochondria of  
840 SW620 cells after its activation. The cells were incubated with PDHH (5  $\mu\text{M}$ ) for 0.5,  
841 1 and 3 h and then stained with Mito-Tracker Deep Red (1  $\mu\text{M}$ ) for another 0.5 h.  
842 Channel 1:  $\lambda_{\text{ex}} = 340\text{-}380 \text{ nm}$ ,  $\lambda_{\text{em}} = \text{LP } 425 \text{ nm}$ ; Channel 2:  $\lambda_{\text{ex}} = 515\text{-}560 \text{ nm}$ ,  $\lambda_{\text{em}}$   
843 = LP 590 nm; Merge: Overlay of channel 1 and channel 2. Scale bar = 20  $\mu\text{m}$ .

844

845 **Figure 7** Fluorescence imaging for therapeutic efficacy of PDHH after its activation  
846 by GSH in SW620 cells. SW620 cells were incubated with PDHH (15  $\mu\text{M}$ ) for 9, 12,

847 18 and 24 h, followed by PI stain. For PDHH, an excitation wavelength  $\lambda_{\text{ex}}= 340\text{-}380$   
848 nm and  $\lambda_{\text{em}} = \text{LP } 425$  nm were used. For PI:  $\lambda_{\text{ex}}= 515\text{-}560$  nm,  $\lambda_{\text{em}} = \text{LP } 590$  nm.  
849 Scale bar = 20  $\mu\text{m}$ .

850

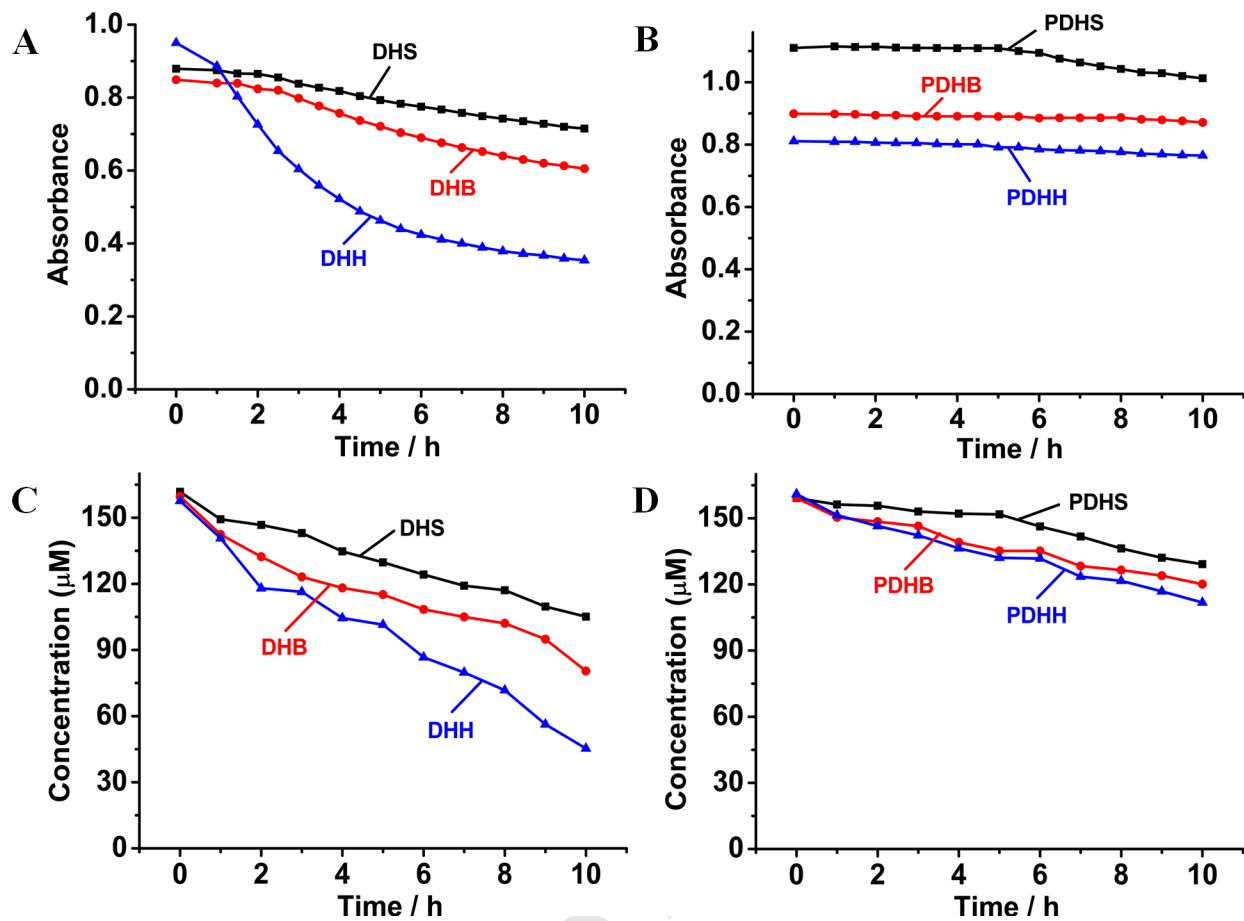
851 **Figure 8** Preferential killing of SW620 over L-02 cells by PDHH *via* a prooxidative  
852 role. (A) The prooxidative mechanism of the catechols. (B) Revision of the  
853 cytotoxicity of PDHH against SW620 by DTT and CAT. (C) Cu(II)-induced  
854 absorption spectral changes of DHH in  $\text{CH}_3\text{CN}/\text{water}$  (1/1, v/v) under air at room  
855 temperature. 1) DHH (20  $\mu\text{M}$ ); 2) DHH (20  $\mu\text{M}$ ) + Cu(II) (20  $\mu\text{M}$ ); 3) DHH (20  $\mu\text{M}$ )  
856 + Cu(II) (20  $\mu\text{M}$ ) + DTT (20  $\mu\text{M}$ ). The inset shows time-dependent absorption  
857 spectral changes of DHH in the presence of Cu(II) for 10 min (interval = 2 min). (D)  
858 Fluorescence images showing the difference of ROS generation induced by 5  $\mu\text{M}$   
859 PDHH between SW620 and L02 cells, and the revision of ROS generation by DTT  
860 and CAT. The cells were pretreated with DTT (400  $\mu\text{M}$ ) or CAT (0.5 mg/mL) for 1 h  
861 and treated with PDHH for 9 h followed by staining with 3  $\mu\text{M}$  DHE for additional 30  
862 min. For DHE:  $\lambda_{\text{ex}} = 515\text{-}560$  nm,  $\lambda_{\text{em}} = \text{LP } 590$  nm. Scale bar for all images = 20  
863  $\mu\text{m}$ . (E) The  $\text{H}_2\text{O}_2$  release from SW620 cells treated with PDHH (2 and 5  $\mu\text{M}$ ) for 6  
864 and 9 h in the absence or presence of 1 h pretreatment with CAT. (F) GSH levels in  
865 SW620 or L02 cells treated with PDHH in the absence or presence of 1 h pretreatment  
866 with DTT or CAT. Each experiment was performed in triplicate. \*\*P<0.01,  
867 \*\*\*P<0.001, vs. the vehicle control; ##P<0.01, ###P<0.001.

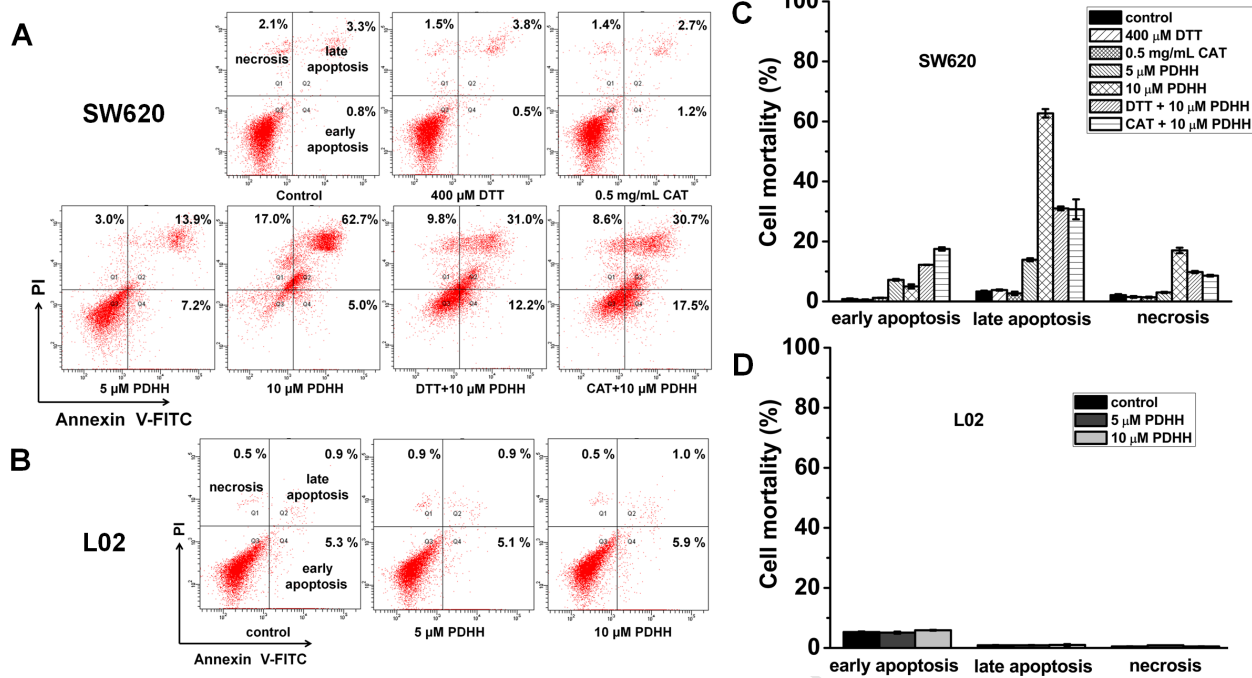
868

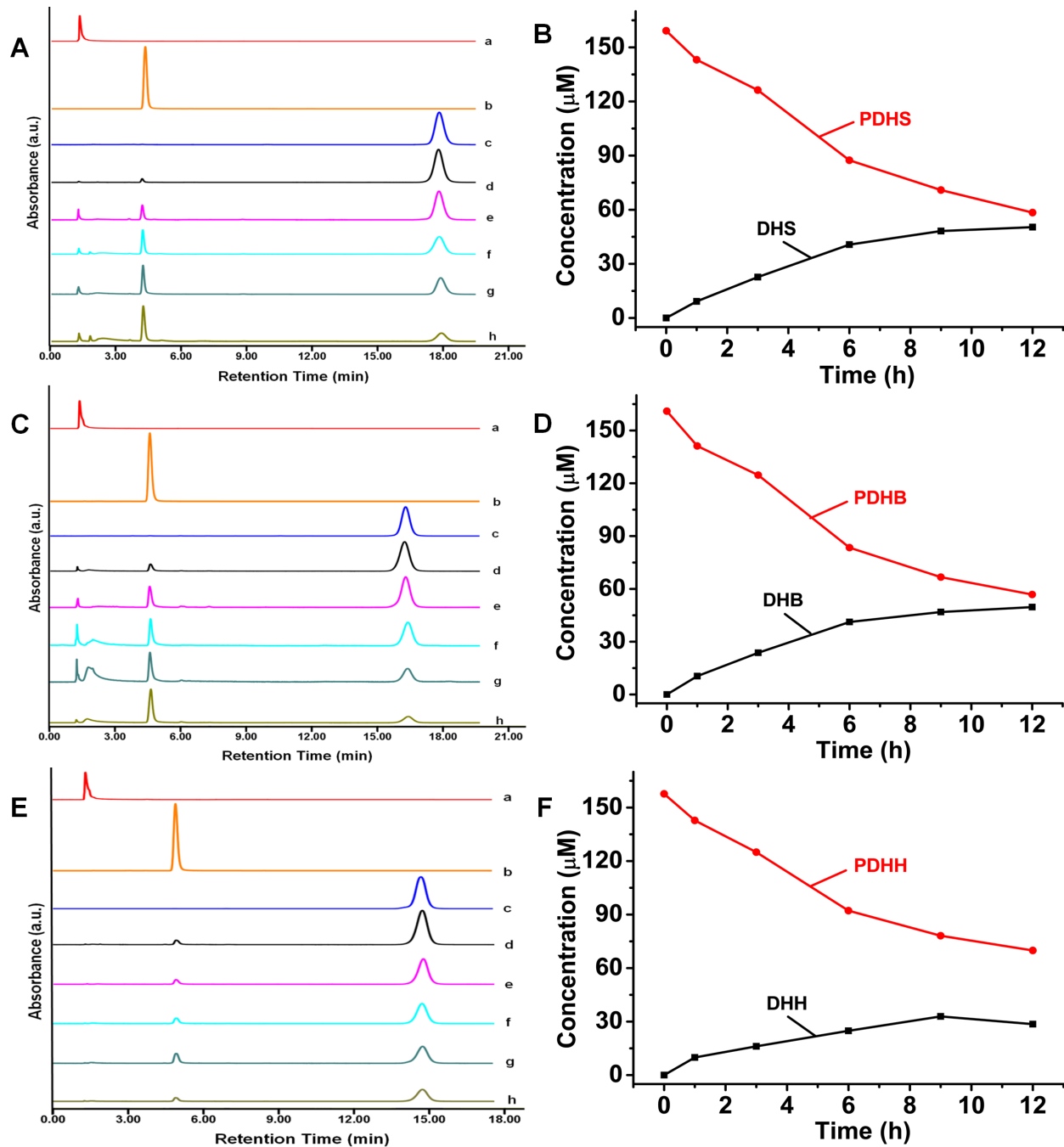
869 **Figure 9** Loss of mitochondrial membrane potential induced by FCCP or PDHH at  
870 the indicated concentrations and time points for SW620 (A) and L02 cells (B). Each  
871 experiment was performed in triplicate. \*\*P<0.01, \*\*\*P<0.001, vs. the vehicle control;  
872 ##P<0.01.

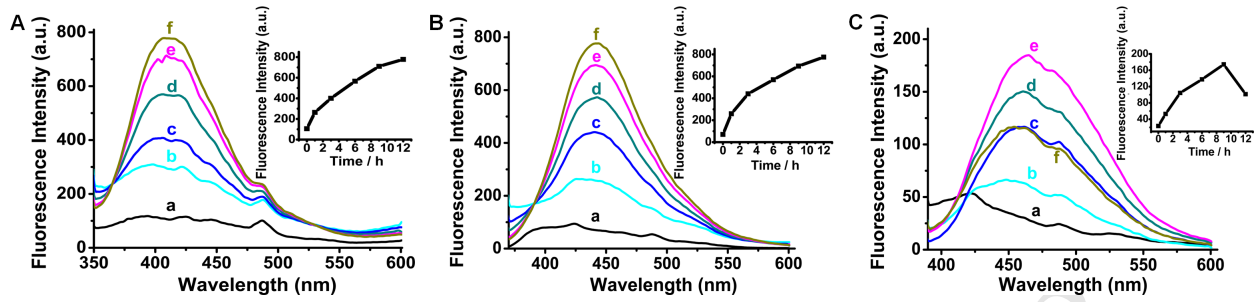
873

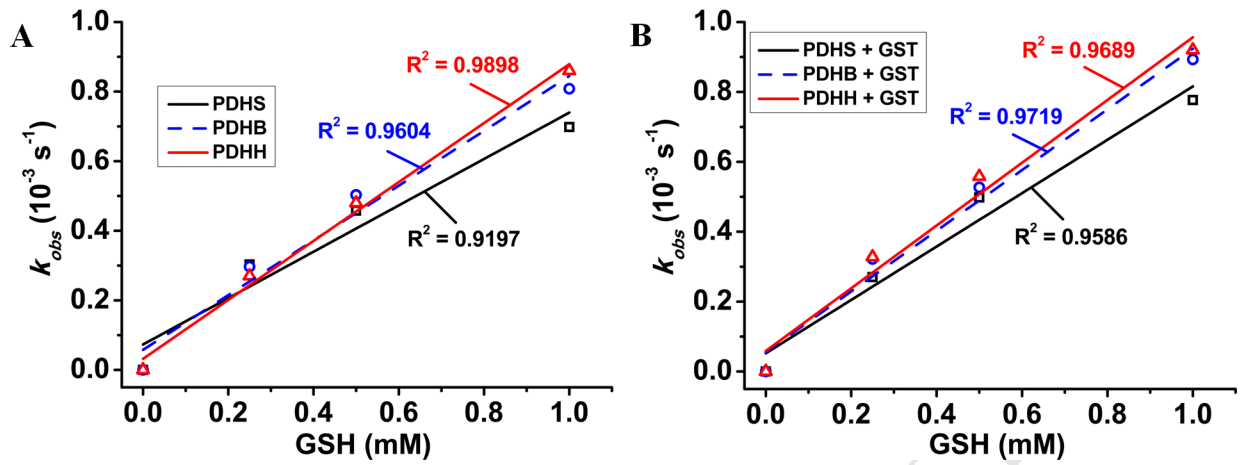
874 **Figure 10** Flow cytometric analyses for apoptotic induction of SW620 cells (A and C)  
875 and normal L02 cells (B and D) after 48 h of treatment with **PDHH** in the absence or  
876 presence of 1 h pretreatment with DTT or CAT. Percentage of cells in early and late  
877 apoptosis and necrosis is indicated in each quadrant. Each experiment was performed  
878 in triplicate and results are shown as the mean  $\pm$  SD in C and D.

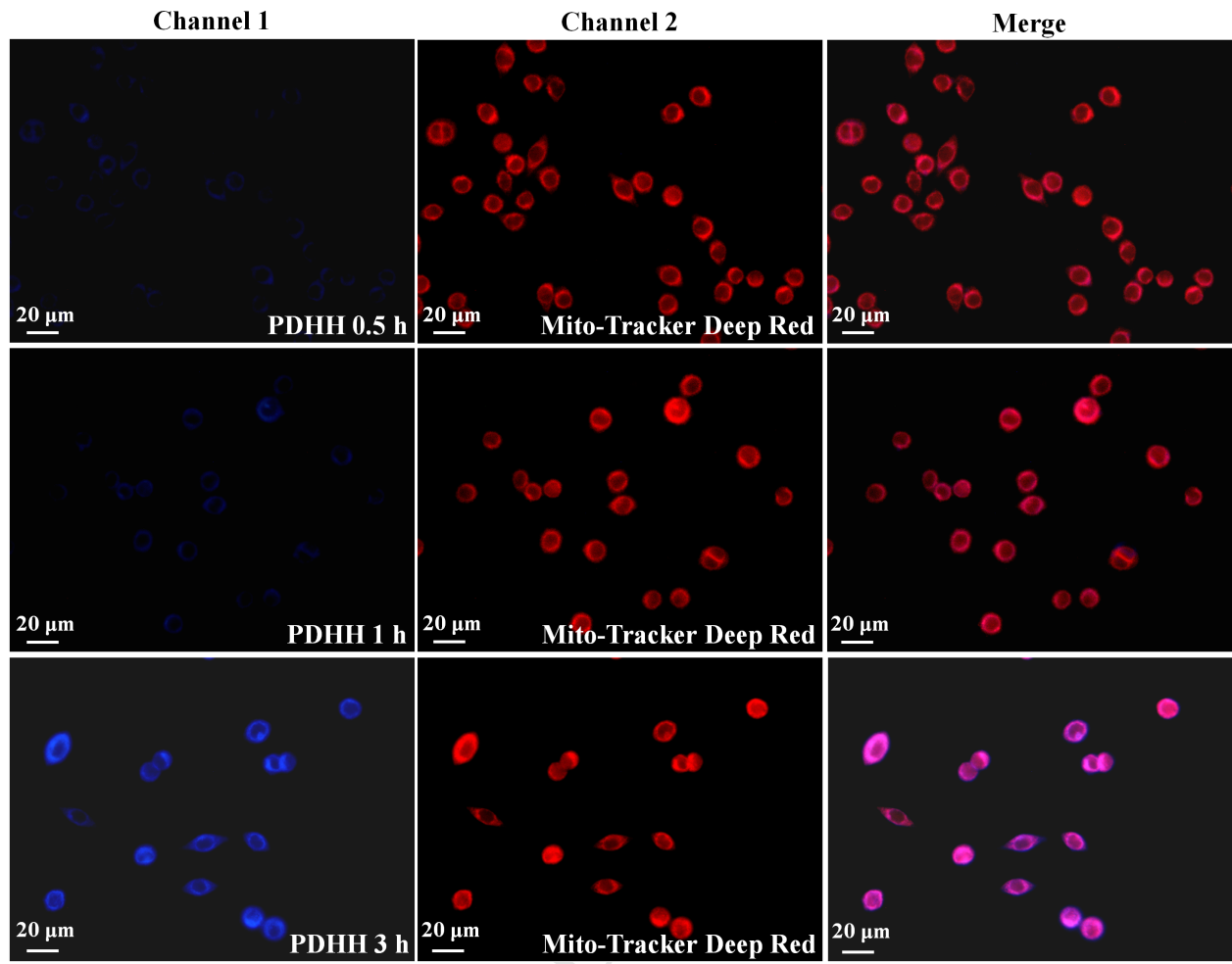


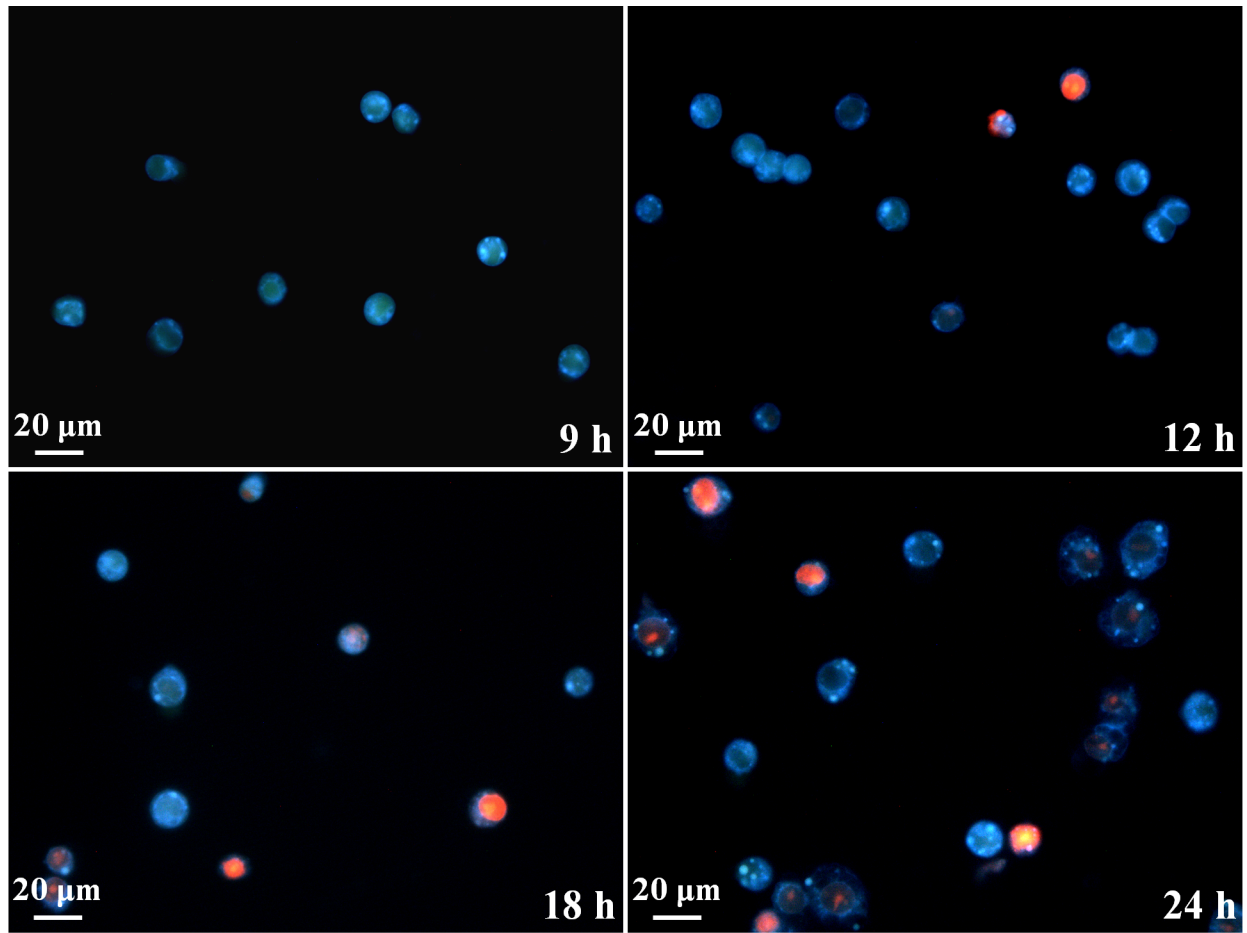


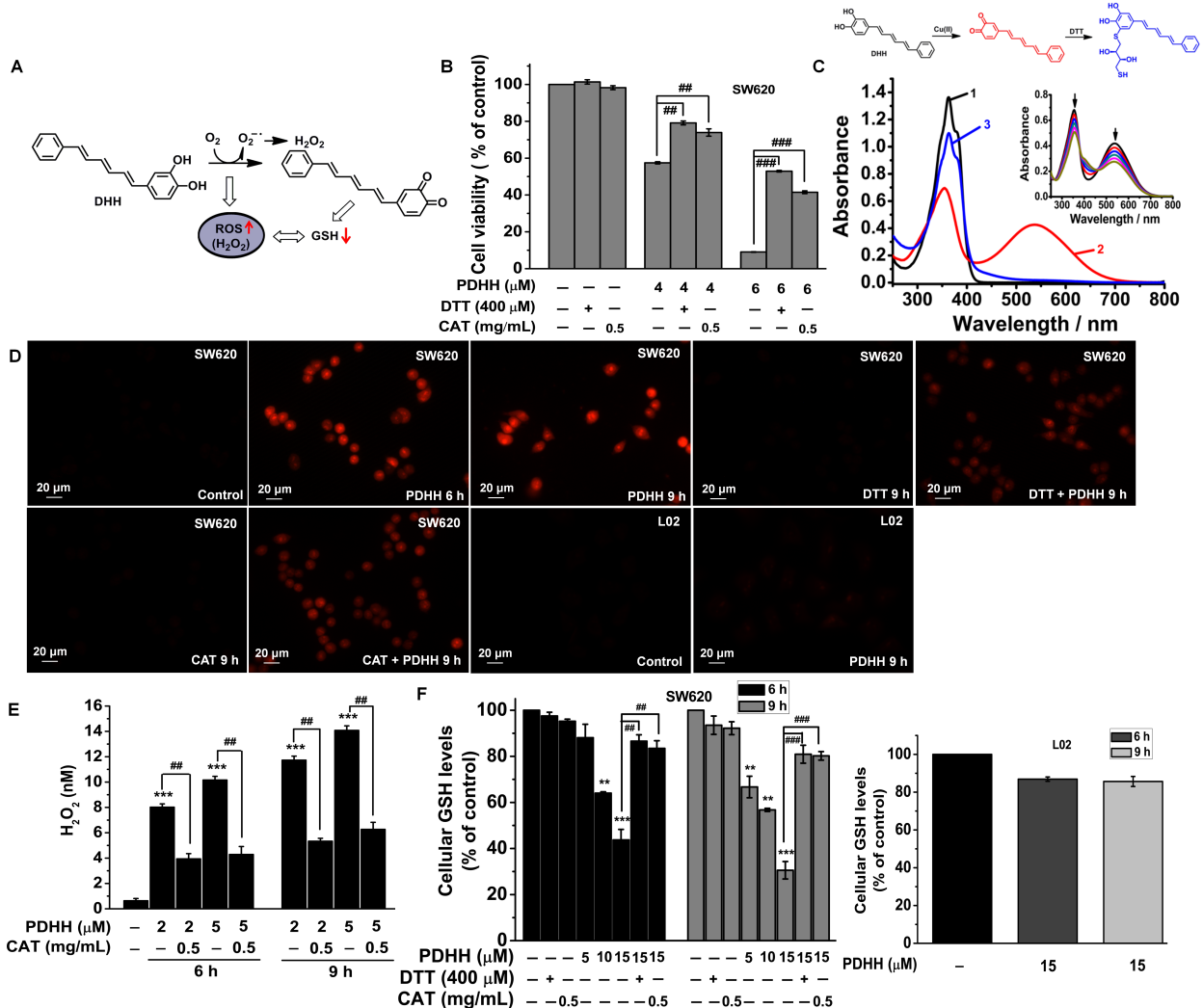


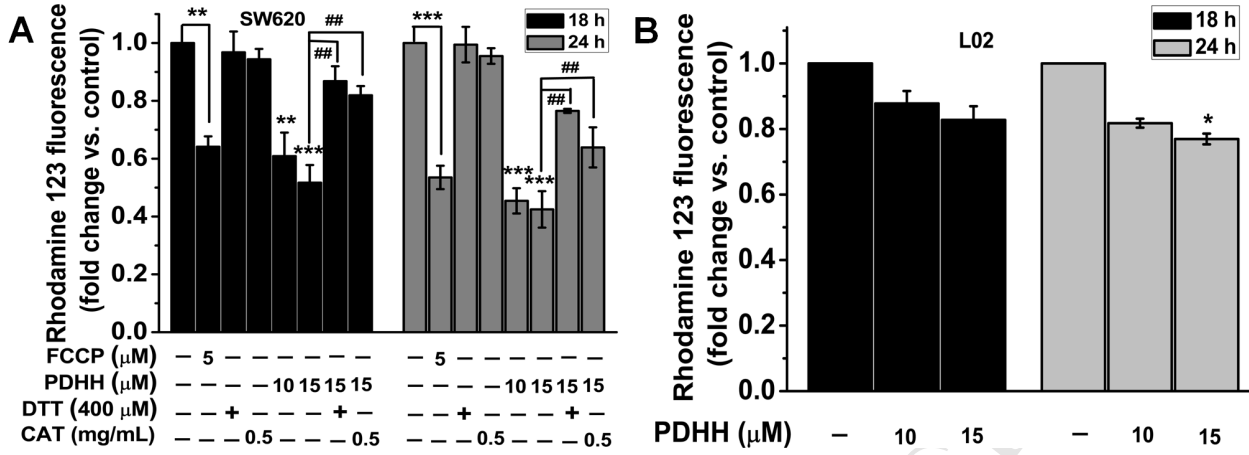


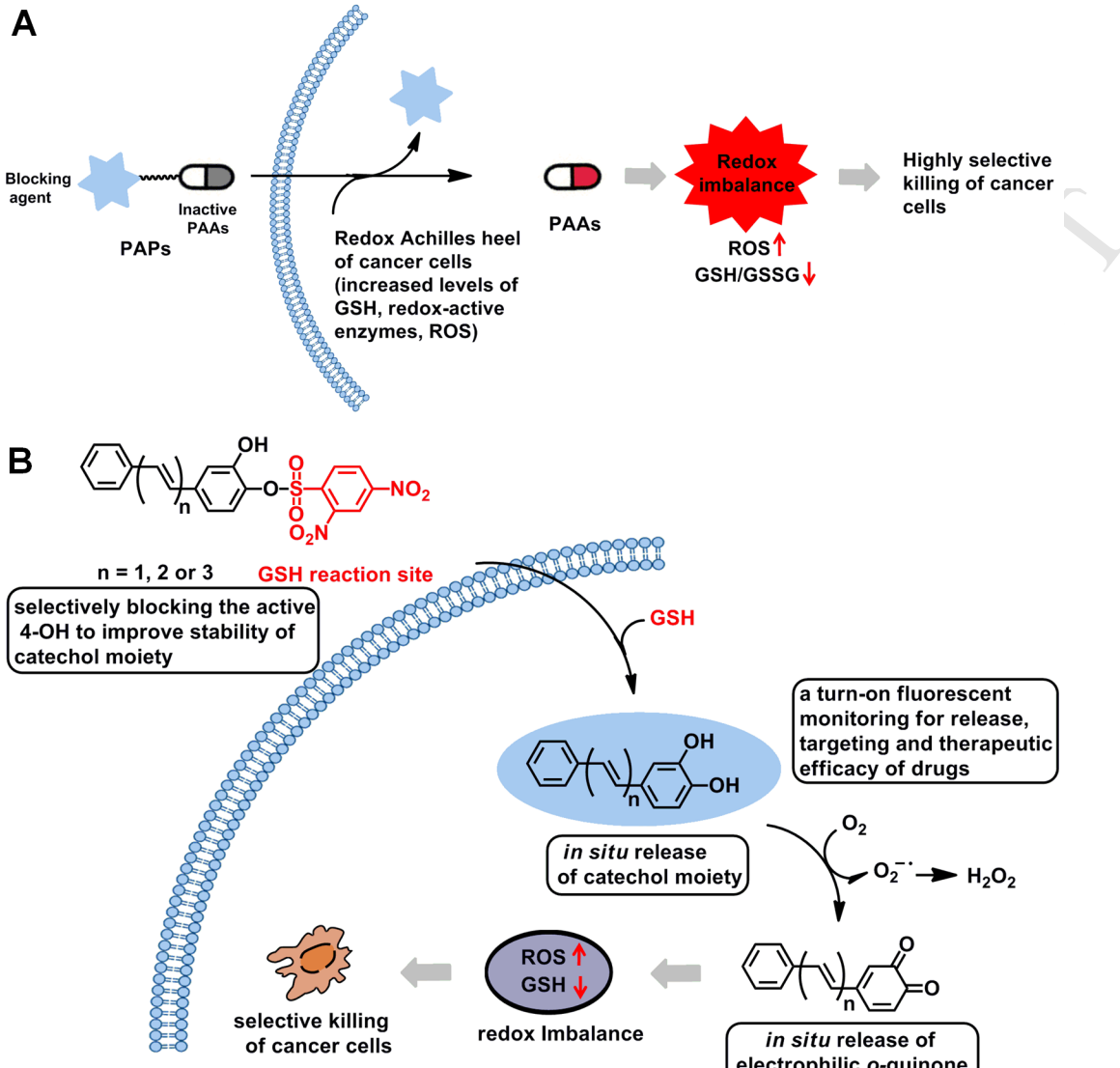


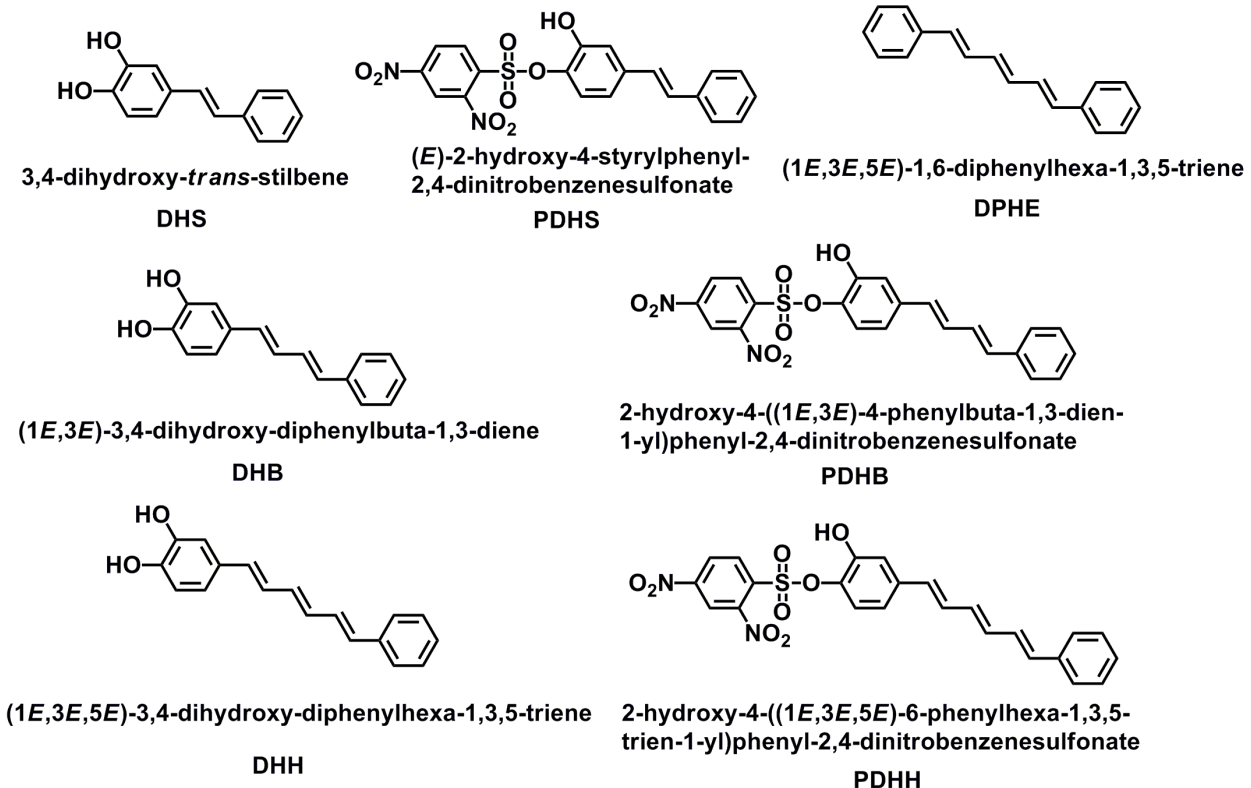


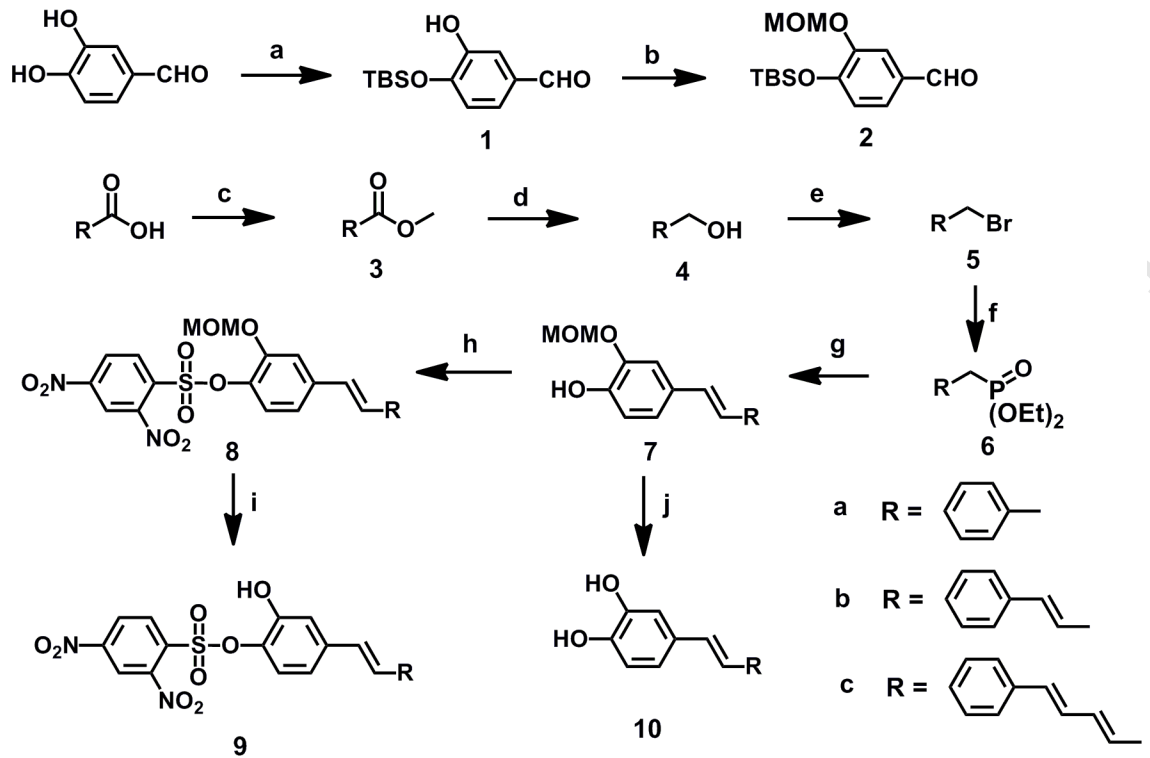


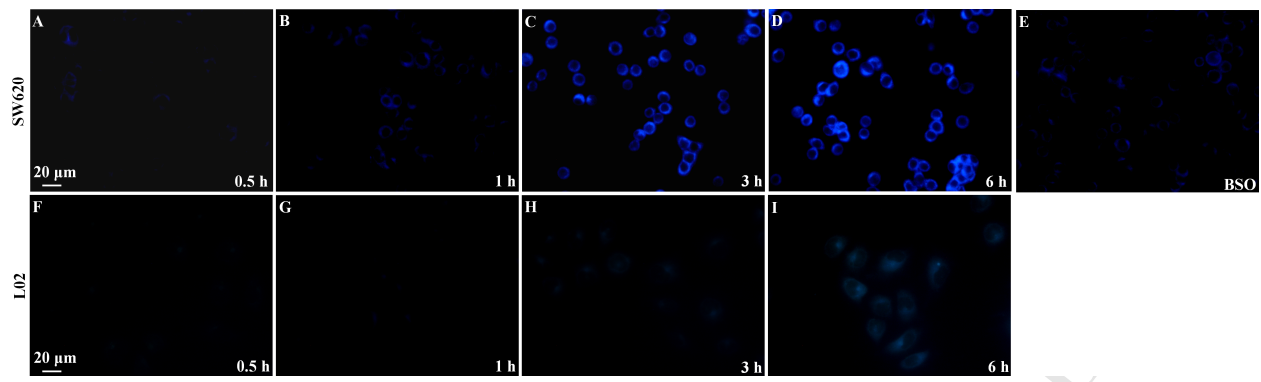












**Highlights**

- Using the GSH-mediated conversion of DNBS to phenols to protect a catechol moiety
- Designing GSH-activated PDHH as a concise theranostic prodrug
- Monitoring for its release, targeting and therapeutic efficacy by a turn-on fluorescent
- Identifying PDHH as a potent prooxidative anticancer prodrug.
- Identifying the diphenylpolyene skeletons as mitochondria-directed groups